Contrib Mineral Petrol (2006) 151: 313–330
DOI 10.1007/s00410-006-0061-z

ORIGINAL PAPER

James L. Crowley · Mark D. Schmitz
Samuel A. Bowring · Michael L. Williams
Karl E. Karlstrom

U–Pb and Hf isotopic analysis of zircon in lower crustal xenoliths from the Navajo volcanic field: 1.4 Ga mafic magmatism and metamorphism beneath the Colorado Plateau

Received: 13 May 2005 / Accepted: 21 December 2005 / Published online: 3 February 2006

Abstract Zircon from lower crustal xenoliths erupted in the Navajo volcanic field was analyzed for U–Pb and Lu–Hf isotopic compositions to characterize the lower crust beneath the Colorado Plateau and to determine whether it was affected by ~1.4 Ga granitic magmatism and metamorphism that profoundly affected the exposed middle crust of southwestern Laurentia. Igneous zircon in felsic xenoliths crystallized at 1.73 and 1.65 Ga, and igneous zircon in mafic xenoliths crystallized at 1.43 Ga. Most igneous zircon has unradiogenic initial Hf isotopic compositions ($\varepsilon_{Hf} = +4.1$ – $+7.8$) and 1.7–1.6 Ga depleted mantle model ages, consistent with 1.7–1.6 Ga felsic protoliths being derived from "juvenile" Proterozoic crust and 1.4 Ga mafic protoliths having interacted with older crust. Metamorphic zircon grew in four pulses between 1.42 and 1.36 Ga, at least one of which was at granulite facies. Significant variability within and between xenoliths in metamorphic zircon initial Hf isotopic compositions ($\varepsilon_{Hf} = -0.7$ to $+13.6$) indicates growth from different aged sources with diverse time-integrated Lu/Hf ratios. These results show a strong link between 1.4 Ga mafic magmatism and granulite facies metamorphism in the lower crust and granitic magmatism and metamorphism in the exposed middle crust.

Communicated by T. L. Grove

J. L. Crowley (✉) · S. A. Bowring
Department of Earth, Atmospheric and Planetary Sciences,
Massachusetts Institute of Technology,
Cambridge, MA 02139, USA
E-mail: jlcrowle@mit.edu
Tel.: +1-617-2531520

M. D. Schmitz
Department of Geosciences, Boise State University,
Boise, ID 83725, USA

M. L. Williams
Department of Geosciences, University of Massachusetts,
Amherst, MA 01003, USA

K. E. Karlstrom
Department of Earth and Planetary Sciences,
University of New Mexico,
Albuquerque, NM 87131, USA

Introduction

The age, composition, and thermal history of the lower crust in southwestern Laurentia are key to understand the processes of Proterozoic lithospheric growth, modification, and reactivation. Continental lithosphere in southwestern Laurentia that formed during the amalgamation of dominantly oceanic elements at 1.8–1.6 Ga (Karlstrom and Bowring 1988; Bowring and Karlstrom 1990) was profoundly modified during granitoid plutonism and metamorphism at 1.4 Ga. Deformation, metamorphism, and $^{40}Ar/^{39}Ar$ cooling dates of 1.4 Ga and younger are recorded over an extensive area (Grambling and Dallmeyer 1993; Hodges et al. 1994; Hodges and Bowring 1995; Karlstrom et al. 1997; Pedrick et al 1998; Shaw et al. 2001), yet a satisfactory explanation for these events that were distant from a plate margin remains elusive. A major limitation to understanding is the uncertainty about the degree to which the lower crust was involved. Karlstrom et al. (2002) suggested that 1.4 Ga granitic magmatism and the distinctive high-velocity lower crust (up to 7.0–7.5 km/s) in southwestern Laurentia resulted from underplating of basalt, but little physical evidence for underplating has been found. Because the highest grade rocks exposed in southwestern Laurentia are relatively high temperature–moderate pressure granulites (700°C, 0.3–0.6 GPa) that were never part of the lower crust, xenoliths entrained in volcanic rocks are the only samples that can be used to establish temporal and petrologic linkages between the exposed middle crust and the hidden lower crust and upper mantle.

Isotopic studies of accessory minerals in xenoliths have revealed much about the formation and thermal history of the lower crust (Rudnick and Williams 1987; Chen et al. 1994; Davis 1997; Moser and Heaman 1997;

Schmitz and Bowring 2001, 2003a, b; Davis et al. 2003; Schmitz et al. 2004), including the timing of protolith crystallization and metamorphism. These studies allowed hypotheses to be tested about the relationship between deep crustal processes and plate tectonic histories manifested in the shallow crustal record. The Navajo volcanic field in the Four Corners area of the Colorado Plateau (Fig. 1) contains abundant crustal xenoliths that have been studied in detail, including geochemistry (Mattie et al. 1997), petrology and thermobarometry (Selverstone et al. 1999), Sm and Nd isotopes (Wendlandt et al. 1993, 1996), and U–Pb zircon geochronology (Condie et al. 1999). Our study was undertaken to gain a better understanding of the evolution of the lower crust beneath the Colorado Plateau and to compare this evolution with the history of basement rocks exposed around the plateau. Moderate-sized (50–100 μm) zircon growth domains were identified through cathodoluminescence (CL) imaging, isolated from adjacent domains by grain fragmentation and air abrasion, dated by the isotope dilution thermal ionization mass spectrometry (IDTIMS) U–Pb method, and then analyzed for Lu–Hf isotopic compositions by multicollector inductively coupled plasma mass spectrometry (MC-ICPMS). This method provides a combination of age and source compositional information from multiple generations of zircon. The results have implications for tectonic models of Proterozoic lithosphere in southwestern Laurentia.

Geological setting

A >1,000 km wide zone of dominantly juvenile crust was accreted to the rifted southern margin of the Wyoming craton between 1.8 and 1.6 Ga (Karlstrom and Bowring 1988, 1993). The orogenic belt has been subdivided into the Yavapai province to the north, Mazatzal to the south (Fig. 1), and Mojave to the west (e.g., Karlstrom and Bowring 1988; Condie 1992; Karlstrom et al. 2002). In general, the Yavapai province consists of 1.8–1.7 Ga juvenile crust deformed and metamorphosed by 1.7 Ga, whereas the Mazatzal is characterized by 1.7–1.6 Ga crust deformed and metamorphosed at ~1.66–1.60 Ga (Karlstrom and Bowring 1988, 1993). Much of the Proterozoic orogenic belt of southwestern Laurentia was strongly affected by the intrusion of granitoid magmas at 1.48–1.32 Ga, with most of the magmatism in New Mexico concentrated at 1.44–1.36 Ga (Karlstrom et al. 2006 and references therein). Regional metamorphism and deformation, associated with this series of magmatic episodes, affected much of northern New Mexico (Pedrick et al. 1998; Read et al. 1999; Williams et al. 1999; Shaw et al. 2001, 2005). The metamorphism was a high temperature–low pressure event (500–550°C, 0.35–0.40 GPa) that was recorded by $^{40}Ar/^{39}Ar$ dates of 1.43–1.35 Ga from rocks around the Colorado Plateau (Karlstrom et al. 1997; Shaw et al. 2001, 2005). Karlstrom et al. (1997, 2002) suggested that the heat for metamorphism was supplied by massive quantities of basalt that underplated the lower crust and induced melting. Evidence for such an event is the regional scale of this crustal heating, the voluminous 1.4 Ga magmatism (~20% of exposed crust in southwestern Laurentia), petrology of the A-type granitoids that suggest a thoeiitic source (Frost and Frost 1997), local association of gabbro, anorthosite, and mafic dikes with 1.4 Ga granite in Colorado and Wyoming, and widespread evidence in 1.4 Ga granitoids for mingled mafic enclaves. Karlstrom et al. (1997) and Shaw et al. (2005) appealed to rapid asthenospheric upwelling similar to lithospheric delamination models of Kay and Kay (1993) to explain the initiation of the basaltic underplating. In some areas, such as the Grand Canyon, 1.4 Ga deformation and metamorphism was considerably less intense (Hawkins et al. 1996; Karlstrom et al. 2006), consistent with exhumation of a laterally segmented orogenic belt (Bowring and

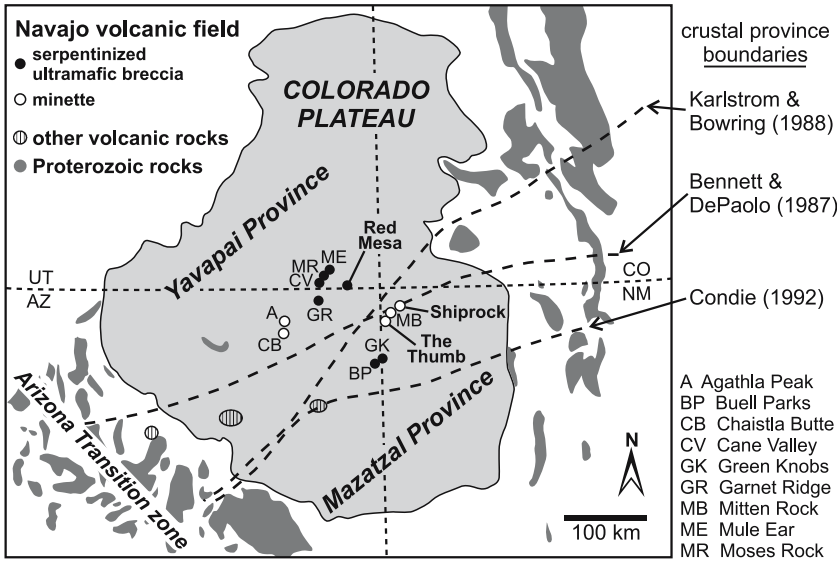

Fig. 1 Map of the Navajo volcanic field, showing the location of diatremes and previously proposed crustal province boundaries

Karlstrom 1990). The highest grade rocks presently at the surface resided at middle crustal depths at ~1.4 Ga. Crustal thickness at ~1.4 Ga is thought to have been "normal" (35–45 km) because thermochronology does not record rapid cooling and uplift following any of the crust forming events, at 1.75–1.65 or 1.45–1.35 Ga (Bowring and Karlstrom 1990; Williams and Karlstrom 1997).

Seismic refraction data acquired by the CD-ROM (Continental Dynamics of the Rocky Mountains) experiment were used to characterize the nature of the lower crust (Karlstrom et al. 2002 and references therein). These data were interpreted by Karlstrom et al. (2002) as delineating a 10–15 km thick, 7.0–7.5 km/s mafic lower crustal layer, the base of which forms the Moho at depths of 40–55 km. The layer was considered to be the net result of diachronous modification of the lithosphere involving magmatic processes from accretion to regional extension at ca 1.1 Ga. Geochronology and isotopic studies of Grt-bearing lower crustal xenoliths from northern Colorado are consistent with a high-velocity mafic lower crust that may be Paleoproterozoic restite, with only minor evidence for magmatism or metamorphism at 1.4 Ga (Karlstrom et al. 2002; Farmer et al. 2005).

The Navajo volcanic field covers >30,000 km^2 in the Four Corners region of the Colorado Plateau (Fig. 1) and is a southward extension of the Colorado Mineral and magmatic belt. It includes more than 80 diatremes (McGetchin et al. 1977; Semken 2003) erupted at 28–19 Ma (Laughlin et al. 1986). Most diatremes are minettes (K-rich lamprophyres) emplaced as magmas (dikes) and gas–solid mixtures (volcanic necks), and others are serpentinized ultramafic microbreccias (kimberlite-like bodies) emplaced as gas–solid mixtures. A wide variety of crustal and mantle xenoliths have been recovered from many of the diatremes [see Table 1 in Selverstone et al. (1999) for summary of lithologies and references]. Xenoliths composed of granitoid and metagranitoid rocks from the middle and upper crusts are common, and those from six diatremes yielded U–Pb zircon crystallization ages corresponding with two of the three main periods of Proterozoic plutonism in southwestern Laurentia, at 1.75–1.70 and 1.45–1.41 Ga (Condie et al. 1999). Mafic xenoliths are also common, being represented by (in order of decreasing abundance) garnet granulite, amphibolite, gabbro, and pyroxene granulite (Mattie et al. 1997). Except for gabbro, none of these xenolith types preserves features that are indicative of protolith. Geochemical analysis suggested that they were derived from dominantly mafic cumulates (Mattie et al. 1997). Metasedimentary schists and gneisses occur in some diatremes, as do eclogites. U–Pb dating of zircon from eclogites and garnetites is consistent with the formation during Late Cretaceous to Tertiary subduction (Usui et al. 2003; Smith et al. 2004; Smith and Griffin 2005).

Selverstone et al. (1999) showed significant differences in the xenoliths across the Navajo field. Xenoliths from diatremes to the northwest (1) represent a variety of rock types, including metasedimentary rocks and eclogites that are absent in diatremes to the southeast; (2) record counterclockwise *P–T* paths with peak temperatures up to 850°C and pressures of >1.0 GPa; (3) underwent complex reaction histories; and (4) suffered variable degrees of hydrous alteration, some of which occurred at 500°C and 0.8–1.2 GPa. Xenoliths from diatremes to the southeast show fewer reaction textures and less alteration and preserve little evidence of their *P–T* evolution. Selverstone et al. (1999) used differences in rock types, *P–T* paths, and alteration histories to suggest that two distinct crustal blocks were juxtaposed along a boundary between the northwest and southeast diatremes. It was proposed that a crustal block to the southeast (Mazatzal province) was thrust beneath a block to the northwest (Yavapai province) based on the assumption that eclogitic metamorphism and hydrous alteration occurred during the accretion and are only recorded in xenoliths from the northwest diatremes. This subduction at the southwestern margin of Laurentia was thought to have occurred at 1.75–1.70 Ga. Other studies have also proposed boundaries between crustal provinces beneath the Colorado Plateau in the vicinity of the Navajo field based on a variety of evidence (Silver 1965; Bennett and DePaolo 1987; Karlstrom and Bowring 1988; Condie 1992; Karlstrom et al. 2002, 2006) (Fig. 1).

Nd whole rock model ages of 1.98–1.63 Ga were obtained from lower crustal granulite and garnet amphibolite xenoliths from four diatremes, similar to ages from upper crustal xenoliths and exposed granitoids (Wendlandt et al. 1993). Sm–Nd garnet-whole rock dates of 1,345 ± 10 Ma obtained from three lower crustal granulite and amphibolite xenoliths from three diatremes (Wendlandt et al. 1996) were interpreted as cooling ages following the 1.4 Ga crustal thermal maximum, which presumably was related to the 1.4 Ga regional metamorphism. Wendlandt et al. (1996) considered the 1.4 Ga thermal event to be associated with intracrustal melting and intrusion of 1.4 Ga granitoid rocks. Selverstone et al. (1999) questioned whether these xenolith isotopic data indicate a distinct metamorphic event at 1.4 Ga and suggested that the region may have simply undergone slow cooling following initial metamorphism and deformation associated with collisional assembly at ~1.7 Ga.

Analytical methods

Garnet- and pyroxene-bearing xenoliths that appeared to be from the middle and lower crusts were collected from The Thumb, Red Mesa, and Shiprock diatremes (Fig. 1). Sixteen xenoliths that varied from 0.2 to 2 kg were processed for heavy minerals. Most xenoliths yielded 10–65 zircon grains that were >100 μm, and many of these were large (200–300 μm), clear, colorless, smooth, subequant, anhedral grains. The grains were mounted in epoxy, polished until their centers were exposed, and imaged for CL using a JEOL 733

Superprobe with an accelerating voltage of 15 keV, a beam current of 3–30 nA, and the secondary electron detector mounted in place of the optical microscope ocular. CL imaging revealed a variety of internal zoning patterns (Fig. 2). Zoning was difficult to discern in grains with domains of strongly contrasting brightness (typically dark cores and bright rims). For such grains, images were first collected at a low beam current to optimize visualization of zoning in the rims, and then the beam current was increased to allow zoning in the cores to become apparent.

Electron microprobe analyses were performed on polished thin sections at the University of Massachusetts on a Cameca SX50 electron microprobe, at 15 kV and 15 nA sample current using natural silicate standards. Wavelength dispersive high-resolution compositional maps were made of individual metamorphic minerals (Grt, Cpx, Hbl, Pl) (abbreviations after Kretz 1983) and matrix domains to evaluate compositional zoning. Quantitative point and traverse locations were selected from compositional maps in such a way as to analyze petrologically significant compositions (i.e., core, near-rim, rim, etc.). Analyses were reduced first using the online PAP routine (Pouchou and Pichoir 1985) and then refined using the Datcon software (M.L. Williams, unpublished). Zircon was located in thin sections with Mg and Zr maps made in stage-scan mode, and CL images were obtained to compare zoning characteristics with zircon in the mineral separates.

Zircon from eight xenoliths (five from Red Mesa, two from The Thumb, and one from Shiprock) was analyzed for U–Pb and Lu–Hf isotopes. Grains selected for analysis generally were those with the largest homogeneous growth domains that represented the different

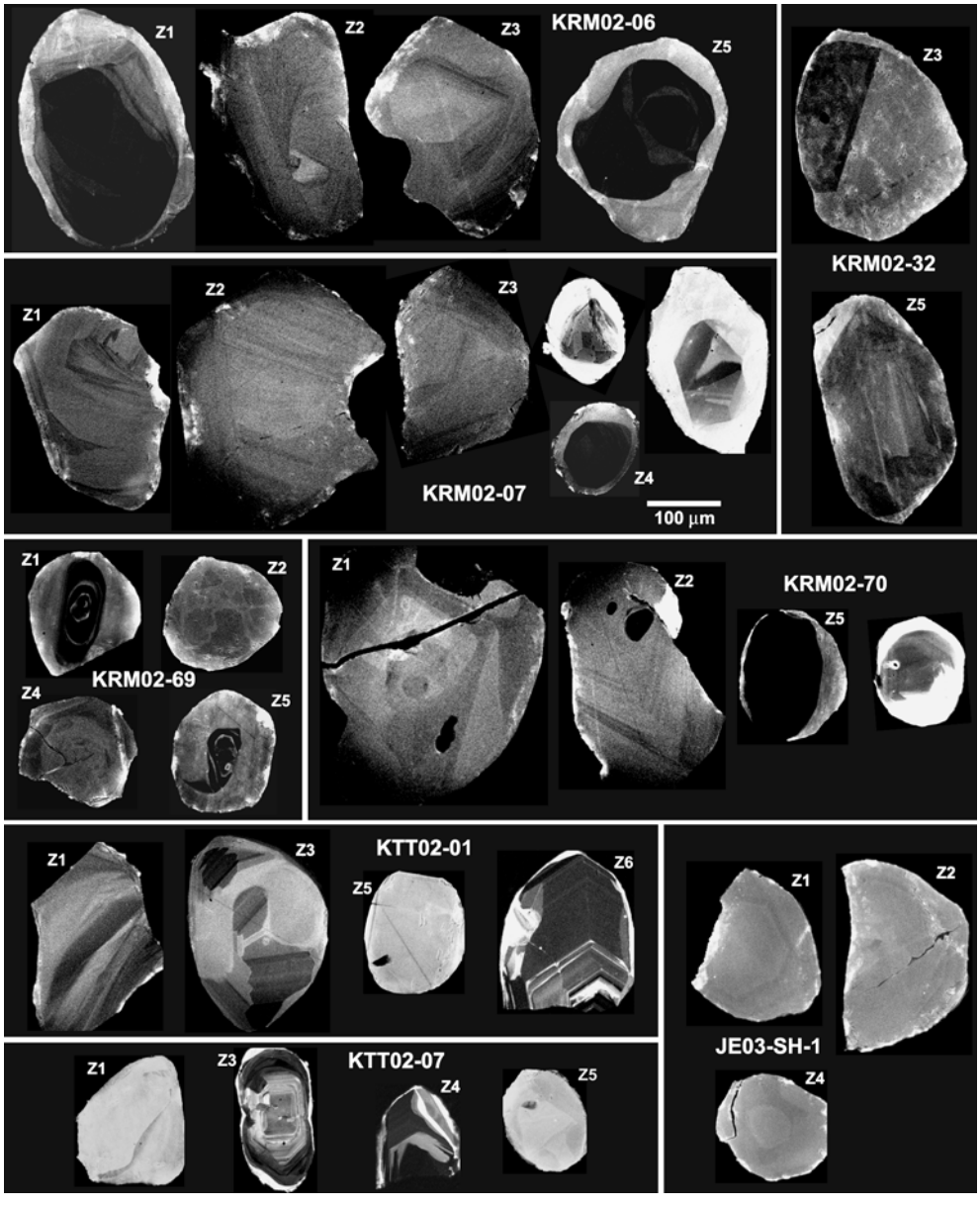

Fig. 2 Cathodoluminescence (*CL*) images of zircon. Grains with labels were removed from the grain mount, fragmented, air-abraded, and dated (Table 2, Figs. 4, 6). Differences in brightness in CL images are related to differences in U concentration, concentrations of other trace elements, and structural parameters such as crystallinity. *Scale bar* applies to all grains

zoning types. We attempted to isolate zircon growth domains by breaking grains that were CL imaged into moderate-sized fragments (50–100 μm, 2–10 fragments per grain). The outer parts of the fragments were removed with air abrasion (Krogh 1982). A problem with this technique is that the boundaries between growth domains were not planes of weakness, and thus the grains did not typically break along them; U–Pb data that show many of the fragments were mixtures of growth domains. The modest spatial resolution of this technique is offset by the high age precision of the IDTIMS method that allows for distinguishing zircon growth episodes that occurred only a few million years apart, in those cases where growth domains were successfully isolated.

U–Pb geochronology followed methods of Schoene et al. (2006). Dates referred to are $^{207}Pb/^{206}Pb$ dates of concordant analyses [i.e., those with $^{207}Pb/^{235}U$ and $^{206}Pb/^{238}U$ dates that agree within analytical and U decay constant errors of Steiger and Jäger (1977)], unless otherwise noted. Errors are reported at $\pm 2\sigma$. Discordia lines in three samples were fitted with a York (1969) regression. Uncertainties on the intercept ages include U decay constant errors of Steiger and Jäger (1977); ignoring these errors reduces the uncertainty by 75% in most cases.

To determine zircon Hf isotopic compositions, 3 M HCl washes from U–Pb anion columns were spiked with a mixed ^{176}Lu–^{178}Hf tracer, fluxed overnight in 6 M HCl–0.1 M HF, dried, redissolved in 1 M HCl–0.1 M HF and Hf quantitatively separated from REEs on a single 1 ml or 100 μl c.v. cation exchange column modified after the first column of Patchett and Tatsumoto (1980). Hf and Lu isotope compositions were measured on the P54 MC-ICPMS at the Department of Terrestrial Magnetism, Carnegie Institution of Washington. All analyses and washouts utilized 1 M HNO_3 (Lu) or 1 M HNO_3–0.05 M HF (Hf) solutions through an MCN-6000 desolvating nebulizer. Hf isotope ratios were measured in static mode on Faraday cups in fifty 10 s integrations, with ^{178}Hf signals $> 0.5\times10^{-11}$ A. Hf isotope ratios were renormalized with an exponential fractionation law to $^{179}Hf/^{177}Hf = 0.7325$; reported $^{176}Hf/^{177}Hf$ ratios were bias corrected relative to the accepted JMC-475 value of 0.282160. Unlike other types of samples, Lu and Yb were not separated prior to analysis; mass fractionation of the Lu isotope ratio was corrected with an exponential law using the mass bias in $^{173}Yb/^{174}Yb$ normalized to a value of 0.5075, and the ^{176}Yb isobaric interference was corrected using a value of $^{173}Yb/^{176}Yb = 0.7844$. Despite the large ^{176}Yb isobar correction (measured $^{174}Yb/^{175}Lu$ ranging from 0.5 to 1.0), this method was sufficient to reproduce the true $^{176}Lu/^{175}Lu$ values in similarly Yb-doped solutions of both natural and spiked Lu samples to within $\pm 1\%$ (2σ), an adequate precision given the very low $^{176}Lu/^{177}Hf$ ratios of zircon.

For whole rock isotopic analysis, 100 mg powder was spiked with mixed ^{149}Sm–^{150}Nd and ^{176}Lu–^{178}Hf tracers, dissolved with 5 ml 29 M HF + 15 M HNO_3 (3:2) in Parr pressure vessels at 200°C for 72 h, dried twice with 1 ml of 15 M HNO_3, and redissolved in 5 ml 6 M HCl at 120°C for 48 h. Resulting clear solutions were dried and redissolved in 5 ml 1 M HCl + 0.1 M HF at 120°C overnight. HF, heavy rare earth elements (REEs), and light REEs were separated sequentially by standard cation exchange chemistry (initial elution of Hf in 1 M HCl + 0.1 M HF, rinsing of major cations with 2.5 M HCl, followed by elution of REEs in two aliquots of 4 M HCl on 6 mm i.d. × 20 cm columns of AG-50W-X8 resin, H^+ form, 200–400 mesh); Sm and Nd were separated by cation exchange in 0.2 M *a*-bishydroxybutyric (methylactic) acid on 2 mm i.d. × 10 cm columns of AG-50W-X8 resin, $(NH_4)^+$ form, 200–400 mesh. Sm and Nd isotopes were measured on the P54 MC-ICPMS in static and dynamic Faraday modes, respectively. Instrumental mass fractionation of Sm and Nd isotopes was corrected with an exponential law relative to $^{146}Nd/^{144}Nd = 0.7219$ and $^{152}Sm/^{147}Sm = 1.783$. The $^{143}Nd/^{144}Nd$ ratio is reported as spike stripped and bias corrected relative to the accepted value of JNdi-1 standard (0.512102). Lu and Hf were separated from whole rock solutions on the cation column described previously. Hf was further purified by the method of Muenker et al. (2000) on 6 mm i.d. × 3.5 cm columns of Eichrom Ln-spec resin (HDEHP-coated resin, 100–200 mesh); for whole rocks, Lu was separated from the bulk of Yb by elution with 2.5 M HCl on 4 mm i.d. × 7.2 cm columns of Eichrom Ln-spec resin. Lu and Hf isotopes were measured on the P54 MC-ICPMS in static Faraday mode. Instrumental mass fractionation of Hf isotopes was corrected with an exponential law relative to $^{179}Hf/^{177}Hf = 0.7325$. The $^{176}Hf/^{177}Hf$ ratio is reported as spike stripped and bias corrected relative to the accepted value of the JMC-475 standard (0.282160). Mass fractionation of the $^{176}Lu/^{175}Lu$ ratio was corrected using the mass bias in $^{173}Yb/^{174}Yb$ normalized to a value of 0.5075, and the ^{176}Yb isobaric interference was corrected using a value of $^{173}Yb/^{176}Yb = 0.7848$; this procedure accurately reproduced the isotope composition of Yb-doped normal and spiked Lu standards.

Mineralogy and thermobarometry

Xenoliths were classified into mafic granulites (abundant Hbl with minor Grt and Cpx) and felsic granulites (dominated by Qtz and Pl with minor Grt, Cpx, and Hbl). Xenoliths from Red Mesa show retrograde textures, with Hbl after Cpx, white mica and Zo after Pl, and Chl after Grt. In contrast, primary mineralogy was generally retained in xenoliths from The Thumb and Shiprock. Four of the five xenoliths from Red Mesa are non-foliated Grt-bearing mafic granulites with similar mineralogy and grain size, and the other is a non-foliated Grt-bearing felsic granulite. Two xenoliths from

The Thumb are moderately foliated felsic granulites, and a xenolith from Shiprock is a foliated Grt-bearing mafic granulite.

Three xenoliths from The Thumb were selected for electron microprobe analysis based on the high preservation of primary mineralogy. Representative mineral compositions are shown in Table 1. Grt is generally $Alm_{46–55}$, $Pyr_{23–37}$, $Grs_{16–23}$. Small crystals are generally unzoned and larger crystals display a subtle trend toward increasing X_{Mg} and X_{Ca} from core to rim. Rims generally display decreasing X_{Mg} and (further) increasing X_{Ca}, interpreted as representing diffusional re-equilibration (probably with Pyx). Cpx has an Mg-ratio of 65–75, a Di component of 35–40%, and a minor Jd component. Cpx is generally unzoned except for a small increase in X_{Mg} near rims, interpreted as resulting from diffusional exchange with Grt. Pl generally has unzoned cores and decreasing X_{An} near rims. The increase in Ab content is interpreted as reflecting the growth of Grt (and Cpx) in these samples. Hbl is characterized by heterogeneous but increasing Mg ratios from inner core (~0.66) to outer core (~0.75) and by broad rims with nearly constant Mg-number. The compositions of the broad rims are interpreted as reflecting near-peak metamorphic conditions.

Compositional analyses were chosen to best represent peak metamorphic conditions. Grt compositions were taken at the point of maximum X_{Mg} just inward from rim reversals, interpreted as reflecting late diffusional re-equilibration. Core compositions were generally used for Cpx and Hbl. Like Grt rims, these core compositions probably reflect some diffusional re-equilibration, but because the amount of zoning is small, all compositions give essentially the same results. Pl compositions were generally taken at maximum X_{Ab} (near rim). X_{Ab} probably increases with Grt growth and because diffusion is extremely slow in plagioclase, rim compositions are interpreted as representing peak conditions. Equilibria were characterized using the TWQ software (Berman 1991; Berman and Brown 1992) and database BA95 (Berman and Aranovich 1996). In general, independent reactions were chosen to correspond to Grt–Pyx or Grt–Hbl exchange thermometers and Grt–Cpx–Pl (or

Table 1 Representative compositions of minerals in xenoliths from The Thumb

	KTT02-01			KTT02-11			KTT02-35			
	Grt	Pl	Pyx	Grt	Pl	Pyx	Grt core	Pl core	Pyx	Hbl ave.
Wt %										
SiO_2	38.86	61.28	51.96	38.87	56.87	50.97	39.78	58.41	51.82	40.19
TiO_2			0.33			0.55	0.03		0.38	2.23
Al_2O_3	21.30	24.75	3.63	21.54	26.51	4.91	22.00	27.49	4.73	14.75
FeO	26.66	0.06	9.41	23.31	0.26	8.09	22.05	0.03	5.79	10.26
MnO	0.94		0.08	0.74		0.04	0.50		0.04	0.05
MgO	6.56		12.34	6.46		12.21	10.37		13.67	13.13
CaO	6.53	6.10	19.51	8.74	8.77	21.71	6.32	9.26	22.50	11.66
Na_2O		7.92	1.38		6.28	1.15		6.04	1.18	1.78
K_2O		0.29			0.46			0.31		2.22
Cr_2O_3			0.05			0.05			0.15	0.21
Total	100.84	100.40	98.68	99.65	99.15	99.68	101.04	101.55	100.27	96.47
Cations										
Si	3.00	2.71	1.96	3.01	2.58	1.90	2.99	2.58	1.91	6.01
Ti			0.01			0.02	0.00		0.01	0.25
Al	1.94	1.29	0.16	1.97	1.42	0.22	1.95	1.43	0.21	2.60
Fe	1.72	0.00	0.30	1.51	0.01	0.25	1.39	0.00	0.18	1.28
Mn	0.06		0.00	0.05		0.00	0.03		0.00	0.01
Mg	0.76		0.69	0.75		0.68	1.16		0.75	2.93
Ca	0.54	0.29	0.79	0.73	0.43	0.87	0.51	0.44	0.89	1.87
Na		0.68	0.10		0.55	0.08		0.52	0.08	0.52
K		0.02			0.03			0.02		0.42
Cr			0.00			0.00			0.00	0.02
End members										
X_{Mg}	0.31		0.70	0.33		0.73	0.46		0.81	0.70
Alm	0.56			0.50			0.45			
Pyr	0.25			0.25			0.38			
Sps	0.02			0.02			0.01			
Grs	0.18			0.24			0.17			
An		0.29			0.42			0.45		
Ab		0.69			0.55			0.53		
Or		0.02			0.03			0.02		
Diop			0.35			0.34			0.37	
Hd			0.15			0.13			0.09	
Jd			0.10			0.08			0.03	

Grt–Hbl–Pl) barometers (see also Williams et al. 2000). Resulting temperatures are 800–850°C and pressures are near 1.3 GPa (Fig. 3), with uncertainties of 75°C and 0.1 GPa.

Thermobarometry was not performed on our Red Mesa samples because of the strong alteration of the primary mineralogy. However, Selverstone et al. (1999) obtained results from a Red Mesa xenolith that is similar to the samples dated here from Red Mesa (primary Grt–Cpx–Pl and several generations of amphibole). Estimates using rim compositions yielded average values of 1.15 GPa and 780°C for Grt–Cpx–amphibole–Pl end members, and 0.95 GPa and 775°C when Pl was omitted. Uncertainties in these calculations are 50°C and 0.15 GPa. We assume similar *P–T* conditions were attained in our Red Mesa samples.

Isotopic results

Red Mesa

Mafic granulites

Most zircon grains in the mafic granulites from Red Mesa are large, clear, colorless to pink, smooth, subequant, and anhedral. Most grains are CL-bright with weak, feathery, curved, and patchy zoning (Fig. 2). About one quarter of the grains have CL-dark cores with concentric, broad oscillatory zoning and sector zoning. The cores are U-richer than the CL-bright domains (300–560 vs. 100–200 ppm in sample KRM02-06) and the cores have higher Th/U (0.35–0.42 vs. 0.21–0.23 in sample KRM02-06). U–Pb zircon dates are concordant within analytical and U decay constant errors (Table 2, Fig. 4). Fragments from grains with CL-dark cores yielded the oldest dates of 1,434–1,420 Ma and fragments from grains without CL-dark cores yielded dates of 1,410–1,360 Ma. Fragments from the same grain typically differ by a few million years (outside of error), suggesting that most grains are composed of multiple growth domains.

In sample KRM02-06, Hf isotopic compositions of four different grains were analyzed (Table 3, Fig. 5), including multiple fragments of two grains. Three grains with U–Pb dates of ~1,430 Ma yielded variable and relatively unradiogenic values ($\varepsilon_{Hf} = +4.1$–$+7.5$; $T_{DM} = 1.71$ and 1.58 Ga). A 1,406 Ma grain has a more radiogenic composition ($\varepsilon_{Hf} = +10.5$; $T_{DM} = 1.44$ Ga). Lu–Hf and Sm–Nd whole rock analysis yielded ε_{Nd} of $+2.08$ ($T_{DM} = 1.80$ Ga) and ε_{Hf} of $+4.84$ ($T_{DM} = 1.73$ Ga) (Table 4). In sample KRM02-07, two grains were analyzed, including multiple fragments of one grain. The older fragment (1,430 Ma) has a more radiogenic initial composition ($\varepsilon_{Hf} = +7.8$, $T_{DM} = 1.57$ Ga) than the younger fragment (1,415 Ma) ($\varepsilon_{Hf} = +2.4$, $T_{DM} = 1.76$ Ga). An even younger grain (1,399 Ma) has the least radiogenic initial composition ($\varepsilon_{Hf} = +0.4$, $T_{DM} = 1.83$ Ga). In sample KRM02-32, three grains were analyzed, including multiple fragments of one grain. The older fragment (1,400 Ma) yielded a more radiogenic initial composition ($\varepsilon_{Hf} = +6.8$; $T_{DM} = 1.58$ Ga) than the two younger grains (1,387, 1,383 Ma) that had the least radiogenic compositions measured in this study ($\varepsilon_{Hf} = -0.5$ to -0.7; $T_{DM} = 1.85$ Ga). In KRM02-70, compositions of three different grains (1,408–1,394 Ma) varied slightly and correlate inversely with age [ε_{Hf} ranging from $+5.6$ to $+6.6$ ($T_{DM} = 1.63$–1.58 Ga) from oldest to youngest].

Felsic granulite

Xenolith KRM02-69 is a felsic granulite with zircon morphologically similar to that in mafic granulites xenoliths from Red Mesa. Most grains are moderately

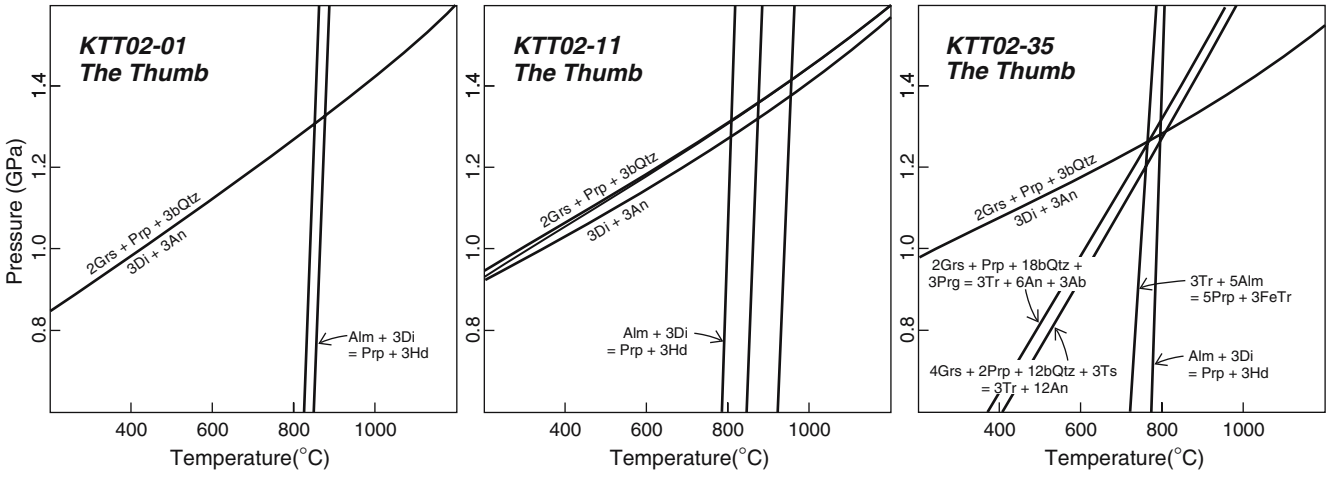

Fig. 3 Plots of estimated pressure–temperature conditions in three xenoliths from The Thumb. Independent reactions were chosen to correspond to Grt–Pyx or Grt–Hbl exchange thermometers and Grt–Cpx–Pl (or Grt–Hbl–Pl) barometers. Results are temperatures of 800–850°C and pressures near 1.3 GPa, with uncertainties on the order of 75°C and 0.1 GPa

Table 2 U–Pb isotopic data

Sample[a]	Weight (μg)[b]	Concentrations					Isotopic ratios									Ages (Ma)			
		U (ppm)	Pb (ppm)	Th/U[c]	Pb_c (pg)[d]	Pb*/Pb_c[e]	$^{206}Pb/^{204}Pb$[f]	$^{208}Pb/^{206}Pb$[g]	$^{206}Pb/^{238}U$[g]	% Err[h]	$^{207}Pb/^{235}U$[g]	% Err[h]	$^{207}Pb/^{206}Pb$[g]	% Err[h]	Corr. coef.	$^{206}Pb/^{238}U$[i]	$^{207}Pb/^{235}U$[i]	$^{207}Pb/^{206}Pb$[i]	% Disc.[j]
KRM02-26 mafic granulite from Red Mesa diatreme																			
Z1a	11.7	332	84.5	0.34	1.2	873.8	54,830	0.103	0.24700	0.05	3.0680	0.06	0.09008	0.04	0.755	1423.0	1424.7	1427.3 ± 0.8	0.3
Z1b	10.2	297	76.4	0.39	1.4	563.8	34,997	0.116	0.24727	0.08	3.0735	0.09	0.09015	0.05	0.860	1424.4	1426.1	1428.7 ± 0.9	0.3
Z2a	5.4	130	31.3	0.21	1.1	157.3	10,230	0.064	0.24262	0.05	2.9781	0.08	0.08902	0.06	0.670	1400.3	1402.0	1404.7 ± 1.1	0.3
Z2b	4.4	201	48.7	0.22	1.0	220.9	14,329	0.066	0.24346	0.05	2.9969	0.08	0.08928	0.06	0.680	1404.7	1406.8	1410.1 ± 1.1	0.4
Z2c	4.6	154	37.2	0.21	1.0	180.1	11,711	0.064	0.24256	0.07	2.9770	0.10	0.08901	0.07	0.693	1400.0	1401.8	1404.4 ± 1.4	0.3
Z3a	9.3	167	41.1	0.22	2.6	154.4	10,011	0.067	0.24607	0.07	3.0486	0.10	0.08986	0.06	0.764	1418.2	1419.9	1422.5 ± 1.2	0.3
Z3b	6.8	163	39.2	0.22	2.0	138.9	9,012	0.067	0.24181	0.06	2.9629	0.08	0.08887	0.06	0.700	1396.1	1398.2	1401.3 ± 1.1	0.4
Z4a	8.7	97	23.6	0.23	1.4	150.8	9,765	0.069	0.24309	0.06	2.9894	0.09	0.08919	0.07	0.694	1402.7	1404.9	1408.2 ± 1.3	0.4
Z4b	5.4	134	32.4	0.22	1.3	138.8	9,010	0.067	0.24280	0.06	2.9821	0.08	0.08908	0.05	0.718	1401.2	1403.1	1405.8 ± 1.0	0.3
Z5a	3.9	565	146.9	0.42	2.0	299.2	18,443	0.125	0.24803	0.05	3.0909	0.06	0.09038	0.04	0.726	1428.3	1430.4	1433.6 ± 0.8	0.4
Z5b	3.6	226	56.0	0.29	1.5	135.8	8,656	0.087	0.24432	0.05	3.0145	0.08	0.08949	0.06	0.621	1409.1	1411.3	1414.6 ± 1.2	0.4
Z5c	3.2	308	78.2	0.34	0.7	370.4	23,255	0.103	0.24636	0.05	3.0547	0.07	0.08993	0.05	0.704	1419.7	1421.4	1424.0 ± 1.0	0.3
KRM02-27 mafic granulite from Red Mesa diatreme																			
Z1a	5.6	195	46.7	0.20	1.7	156.9	10,239	0.060	0.24155	0.06	2.9565	0.08	0.08877	0.06	0.71	1394.7	1396.5	1399.2 ± 1.1	0.3
Z1b	7.1	156	37.3	0.20	2.0	139.9	9,132	0.060	0.24141	0.06	2.9544	0.08	0.08876	0.05	0.74	1394.0	1396.0	1399.0 ± 1.0	0.4
Z2a	5.8	196	47.1	0.21	1.3	212.9	13,838	0.064	0.24231	0.06	2.9732	0.07	0.08899	0.05	0.75	1398.7	1400.8	1404.0 ± 0.9	0.4
Z2b	4.9	238	56.7	0.20	1.7	173.1	11,292	0.061	0.24072	0.08	2.9425	0.10	0.08865	0.06	0.81	1390.4	1392.9	1396.7 ± 1.1	0.4
Z3a	4.2	149	36.1	0.21	1.1	143.3	9,315	0.064	0.24324	0.07	2.9896	0.11	0.08914	0.08	0.68	1403.5	1405.0	1407.2 ± 1.5	0.3
Z3b	2.0	222	52.3	0.20	1.0	107.3	7,013	0.060	0.23816	0.08	2.8989	0.10	0.08828	0.06	0.80	1377.1	1381.6	1388.6 ± 1.1	0.8
Z3c	2.8	101	24.8	0.23	0.9	84.3	5,473	0.068	0.24522	0.08	3.0282	0.12	0.08956	0.08	0.72	1413.8	1414.7	1416.2 ± 1.6	0.2
Z4a	1.0	326	79.9	0.20	1.5	66.6	4,352	0.060	0.24708	0.09	3.0734	0.12	0.09022	0.08	0.75	1423.4	1426.1	1430.1 ± 1.5	0.5
Z4b	0.8	233	57.3	0.26	0.9	53.1	3,423	0.077	0.24485	0.08	3.0209	0.10	0.08948	0.07	0.77	1411.8	1412.9	1414.5 ± 1.3	0.2
KRM02-22 mafic granulite from Red Mesa diatreme																			
Z2	3.1	30	6.9	0.11	2.2	9.8	671	0.033	0.23999	0.32	2.9186	0.42	0.08820	0.26	0.80	1386.6	1386.7	1386.9 ± 4.9	0.0
Z3a	1.2	80	18.5	0.12	1.9	11.7	800	0.036	0.23893	0.55	2.9022	0.62	0.08810	0.27	0.90	1381.1	1382.5	1384.6 ± 5.2	0.2
Z3b	1.2	77	17.8	0.12	1.4	15.4	1,044	0.037	0.23819	0.40	2.8947	0.42	0.08814	0.13	0.95	1377.3	1380.5	1385.5 ± 2.6	0.6
Z4a	3.1	21	4.9	0.11	1.7	9.0	620	0.032	0.23876	0.38	2.8964	0.48	0.08798	0.27	0.83	1380.3	1381.0	1382.0 ± 5.1	0.1
Z4b	2.2	46	10.2	0.09	1.5	14.8	1,015	0.026	0.23248	0.30	2.7927	0.36	0.08712	0.19	0.85	1347.5	1353.6	1363.2 ± 3.6	1.2
Z5a	5.8	28	6.5	0.12	1.1	33.8	2,267	0.037	0.24184	0.14	2.9619	0.18	0.08883	0.10	0.82	1396.3	1397.9	1400.4 ± 2.0	0.3
Z5b	5.2	30	7.2	0.19	0.9	42.2	2,776	0.056	0.24268	0.14	2.9778	0.18	0.08900	0.11	0.80	1400.6	1402.0	1404.1 ± 2.1	0.2
Z7	5.1	39	8.7	0.11	1.0	43.9	2,952	0.032	0.23542	0.12	2.8391	0.18	0.08747	0.14	0.65	1362.8	1365.9	1370.8 ± 2.6	0.6
Z8a	5.0	22	4.9	0.11	2.9	16.8	1,142	0.034	0.23387	0.26	2.8018	0.30	0.08689	0.15	0.88	1354.8	1356.0	1358.0 ± 2.8	0.2
Z8c	2.3	6	1.3	0.10	0.8	16.8	1,146	0.031	0.23409	0.26	2.8141	0.31	0.08719	0.16	0.86	1355.9	1359.3	1364.6 ± 3.1	0.6
KRM02-29 felsic granulite from Red Mesa diatreme																			
Z1a	1.3	125	34.0	0.59	6.3	7.0	430	0.179	0.24948	0.52	3.1375	0.60	0.09121	0.27	0.89	1435.8	1441.9	1451.0 ± 5.2	1.0
Z1b	1.3	191	49.2	0.18	1.0	61.8	4,049	0.054	0.26154	0.08	3.4175	0.10	0.09477	0.07	0.77	1497.7	1508.4	1523.5 ± 1.2	1.7
Z1c	0.9	90	24.3	0.56	1.2	19.0	1,147	0.167	0.24839	0.24	3.1044	0.30	0.09064	0.18	0.81	1430.2	1433.8	1439.1 ± 3.4	0.6
Z2a	3.5	79	25.3	1.48	2.4	36.4	1,794	0.444	0.24393	0.13	3.0108	0.18	0.08952	0.12	0.76	1407.1	1410.4	1415.3 ± 2.2	0.6
Z2b	2.8	90	28.2	1.39	6.5	12.2	623	0.418	0.24054	0.38	2.9454	0.42	0.08881	0.17	0.92	1389.5	1393.7	1400.1 ± 3.2	0.8
Z3	1.5	72	22.3	1.33	1.2	28.4	1,448	0.397	0.24262	0.15	2.9728	0.18	0.08887	0.08	0.88	1400.3	1400.7	1401.3 ± 1.6	0.1
Z4b	2.4	95	26.5	0.82	1.5	42.3	2,389	0.245	0.24187	0.10	2.9628	0.13	0.08884	0.08	0.81	1396.4	1398.1	1400.7 ± 1.5	0.3
Z4c	2.3	57	18.1	1.40	1.0	43.5	2,171	0.419	0.24363	0.11	2.9967	0.13	0.08921	0.08	0.82	1405.5	1406.8	1408.7 ± 1.5	0.2
Z5a	3.5	72	21.2	1.11	0.8	94.9	5,014	0.332	0.24181	0.11	2.9594	0.13	0.08876	0.07	0.83	1396.1	1397.3	1399.0 ± 1.4	0.2
Z5b	2.8	152	40.0	0.29	0.8	138.8	8,821	0.086	0.25886	0.08	3.3423	0.10	0.09364	0.06	0.81	1484.0	1491.0	1500.9 ± 1.1	1.1
Z5c	1.4	48	12.5	0.60	0.7	26.8	1,603	0.177	0.24096	0.15	2.9363	0.20	0.08838	0.11	0.81	1391.7	1391.3	1390.8 ± 2.2	−0.1

Table 2 (Contd.)

KRM02-20 mafic granulite from Red Mesa diatreme																		
Z1a	6.8	27	6.3	0.19	2.2	20.0	1,327	0.058	0.24140	0.36	2.9584	0.39	0.08888	0.14	0.93	1394.0	1397.0	1401.6 ± 2.7	0.5
Z1b	7.4	38	9.1	0.19	1.6	43.2	2,838	0.057	0.24279	0.09	2.9826	0.11	0.08910	0.06	0.82	1401.2	1403.2	1406.2 ± 1.2	0.4
Z2a	10.4	99	23.8	0.27	1.9	132.8	8,527	0.079	0.24008	0.09	2.9289	0.10	0.08848	0.06	0.83	1387.1	1389.4	1392.9 ± 1.1	0.4
Z2b	3.3	85	20.6	0.26	2.7	25.1	1,631	0.076	0.24077	0.16	2.9391	0.20	0.08854	0.11	0.84	1390.7	1392.0	1394.1 ± 2.0	0.2
Z3a	2.9	60	14.3	0.23	0.8	48.8	3,171	0.070	0.24087	0.11	2.9402	0.14	0.08853	0.08	0.81	1391.2	1392.3	1394.0 ± 1.5	0.2
Z3b	2.9	68	16.3	0.23	1.7	28.0	1,832	0.069	0.24162	0.12	2.9548	0.15	0.08869	0.08	0.83	1395.1	1396.1	1397.5 ± 1.6	0.2
Z4a	2.8	73	17.7	0.24	1.1	44.6	2,896	0.071	0.24337	0.11	2.9929	0.14	0.08919	0.08	0.79	1404.2	1405.8	1408.3 ± 1.6	0.3
Z4b	2.0	110	26.7	0.22	2.0	26.1	1,712	0.066	0.24345	0.20	3.0007	0.24	0.08939	0.13	0.84	1404.6	1407.8	1412.6 ± 2.5	0.6
Z5	2.1	29	7.0	0.18	1.9	14.4	963	0.054	0.24704	0.23	3.0664	0.28	0.09002	0.14	0.85	1423.2	1424.3	1426.1 ± 2.7	0.2
KTT02-21 felsic granulite from The Thumb diatreme																			
Z1a	4.8	4,145	944.4	0.08	1.2	3627.6	244,091	0.025	0.23822	0.07	2.8932	0.08	0.08808	0.04	0.87	1377.5	1380.1	1384.3 ± 0.8	0.5
Z1b	2.9	3,253	738.7	0.07	3.8	566.6	38,222	0.022	0.23794	0.12	2.8864	0.13	0.08798	0.06	0.90	1376.0	1378.4	1382.1 ± 1.1	0.4
Z3a	8.6	796	185.3	0.07	1.1	1465.0	98,835	0.020	0.24406	0.05	3.0130	0.06	0.08954	0.04	0.75	1407.8	1410.9	1415.7 ± 0.8	0.6
Z3b	4.5	823	190.2	0.07	2.7	316.2	21,353	0.021	0.24244	0.07	2.9777	0.08	0.08908	0.05	0.83	1399.3	1401.9	1405.9 ± 0.9	0.5
Z3c	3.8	620	145.8	0.06	3.6	153.9	10,413	0.018	0.24675	0.06	3.0715	0.08	0.09028	0.05	0.72	1421.7	1425.6	1431.5 ± 1.0	0.7
Z4b	7.1	2,935	679.6	0.09	1.2	3957.4	265,403	0.028	0.24128	0.05	2.9538	0.06	0.08879	0.04	0.77	1393.4	1395.8	1399.6 ± 0.8	0.4
Z4c	3.3	3,659	845.7	0.09	1.2	2298.1	154,193	0.027	0.24093	0.06	2.9449	0.07	0.08865	0.04	0.83	1391.5	1393.5	1396.6 ± 0.8	0.4
Z5b	1.6	602	142.3	0.11	1.0	220.4	14,706	0.034	0.24456	0.05	3.0264	0.07	0.08975	0.06	0.67	1410.4	1414.3	1420.2 ± 1.1	0.7
Z6a	4.0	4,569	1217.0	0.03	0.8	6074.0	409,849	0.010	0.27943	0.06	3.8036	0.07	0.09872	0.04	0.84	1588.5	1593.5	1600.1 ± 0.7	0.7
Z6b	2.8	4,011	996.1	0.04	0.5	7537.3	510,142	0.011	0.26137	0.05	3.3997	0.07	0.09434	0.04	0.80	1496.9	1504.3	1514.9 ± 0.8	1.2
Z6c	3.8	3,487	875.6	0.04	0.8	3241.3	219,401	0.011	0.26422	0.05	3.4627	0.07	0.09505	0.04	0.79	1511.4	1518.8	1529.1 ± 0.8	1.2
KTT02-27 felsic granulite from The Thumb diatreme																			
Z1a	3.3	105	31.0	1.04	1.3	77.2	4,136	0.312	0.24380	0.07	3.0025	0.11	0.08932	0.09	0.63	1406.4	1408.3	1411.0 ± 1.7	0.3
Z1b	2.3	388	104.8	0.38	0.8	314.1	19,480	0.113	0.26029	0.05	3.3742	0.07	0.09402	0.05	0.67	1491.3	1498.4	1508.5 ± 1.0	1.1
Z1c	1.1	389	101.2	0.21	1.2	92.8	6,018	0.063	0.26161	0.07	3.4030	0.09	0.09434	0.05	0.83	1498.1	1505.1	1515.0 ± 0.9	1.1
Z3a	1.3	1,038	273.2	0.10	1.2	290.5	19,315	0.029	0.27170	0.07	3.6540	0.09	0.09754	0.05	0.84	1549.4	1561.4	1577.6 ± 0.9	1.8
Z3b	1.8	834	225.8	0.09	0.7	619.2	41,174	0.026	0.27967	0.05	3.8329	0.07	0.09940	0.04	0.76	1589.7	1599.7	1612.9 ± 0.8	1.4
Z4a	2.1	2,429	663.1	0.01	0.7	1945.9	131,896	0.003	0.28764	0.05	3.9936	0.06	0.10070	0.04	0.77	1629.7	1632.9	1637.0 ± 0.8	0.4
Z4b	2.7	2,406	660.0	0.01	1.3	1416.6	96,047	0.003	0.28897	0.07	4.0265	0.08	0.10106	0.04	0.87	1636.4	1639.6	1643.7 ± 0.8	0.4
Z5a	2.5	297	74.0	0.22	1.0	185.3	12,014	0.065	0.25036	0.07	3.1509	0.08	0.09128	0.05	0.79	1440.3	1445.2	1452.5 ± 1.0	0.8
Z5b	2.0	113	31.3	0.74	0.9	66.0	3,778	0.222	0.24544	0.20	3.0513	0.22	0.09016	0.09	0.92	1414.9	1420.6	1429.0 ± 1.7	1.0
JE03-SH-1 mafic granulite from Shiprock diatreme																			
Z1	2.5	47	13.8	0.98	1.4	24.4	1,337	0.291	0.24565	0.16	3.0336	0.21	0.08957	0.12	0.82	1416.0	1416.1	1416.3 ± 2.2	0.0
Z2a	3.1	77	24.1	1.32	1.1	65.2	3,301	0.395	0.24561	0.12	3.0366	0.14	0.08967	0.07	0.87	1415.8	1416.9	1418.5 ± 1.4	0.2
Z2b	2.9	63	19.1	1.19	1.1	49.9	2,600	0.354	0.24543	0.14	3.0319	0.15	0.08960	0.07	0.90	1414.9	1415.7	1417.0 ± 1.3	0.1
Z3a	7.0	62	18.5	1.06	2.6	50.7	2,714	0.316	0.24550	0.10	3.0346	0.13	0.08965	0.07	0.83	1415.2	1416.4	1418.1 ± 1.4	0.2
Z3b	4.1	61	19.2	1.31	2.0	39.8	2,027	0.390	0.24512	0.15	3.0310	0.18	0.08968	0.09	0.87	1413.3	1415.5	1418.7 ± 1.7	0.4
Z4	2.9	96	24.5	0.42	4.6	15.6	979	0.124	0.24491	0.21	3.0252	0.31	0.08959	0.21	0.74	1412.2	1414.0	1416.7 ± 4.0	0.3

[a] Z1a, Z1b, Z2a, etc., correspond to labels on concordia diagrams (Figs. 4, 6). Fractions are composed of single zircon fragments; letters following the same number are fragments from the same grain
[b] Sample weights are estimated to within 40% using measured grain dimensions and density
[c] Model Th/U ratio calculated from radiogenic $^{208}Pb/^{206}Pb$ ratio and $^{207}Pb/^{206}Pb$ age
[d] Total weight of common Pb
[e] Ratio of radiogenic Pb to common Pb
[f] Measured ratio corrected for spike and fractionation only. Mass fractionation correction of 0.25 ± 0.04%/amu (atomic mass unit) was applied to single-collector Daly analyses (based on daily analysis of NBS-981) and a correction of 0.07%/amu ± 0.04% was applied to Dynamic Faraday–Daly analyses
[g] Corrected for fractionation, spike, blank, and initial common Pb. All common Pb were assumed to be procedural blank. U blank was < 0.1 pg. Measured laboratory blank composition: $^{206}Pb/^{204}Pb = 18.27 \pm 0.1$, $^{207}Pb/^{204}Pb = 15.59 \pm 0.1$, $^{208}Pb/^{204}Pb = 38.12 \pm 0.1$ (2σ)
[h] Errors are 2σ, propagated using the algorithms of Ludwig (1980)
[i] Age calculations are based on the decay constants of Steiger and Jäger (1977). Error in the $^{207}Pb/^{206}Pb$ age is 2σ
[j] Discordance (%) = $100 - [100 \times (^{206}Pb/^{238}U \text{ age})/(^{207}Pb/^{206}Pb \text{ age})]$

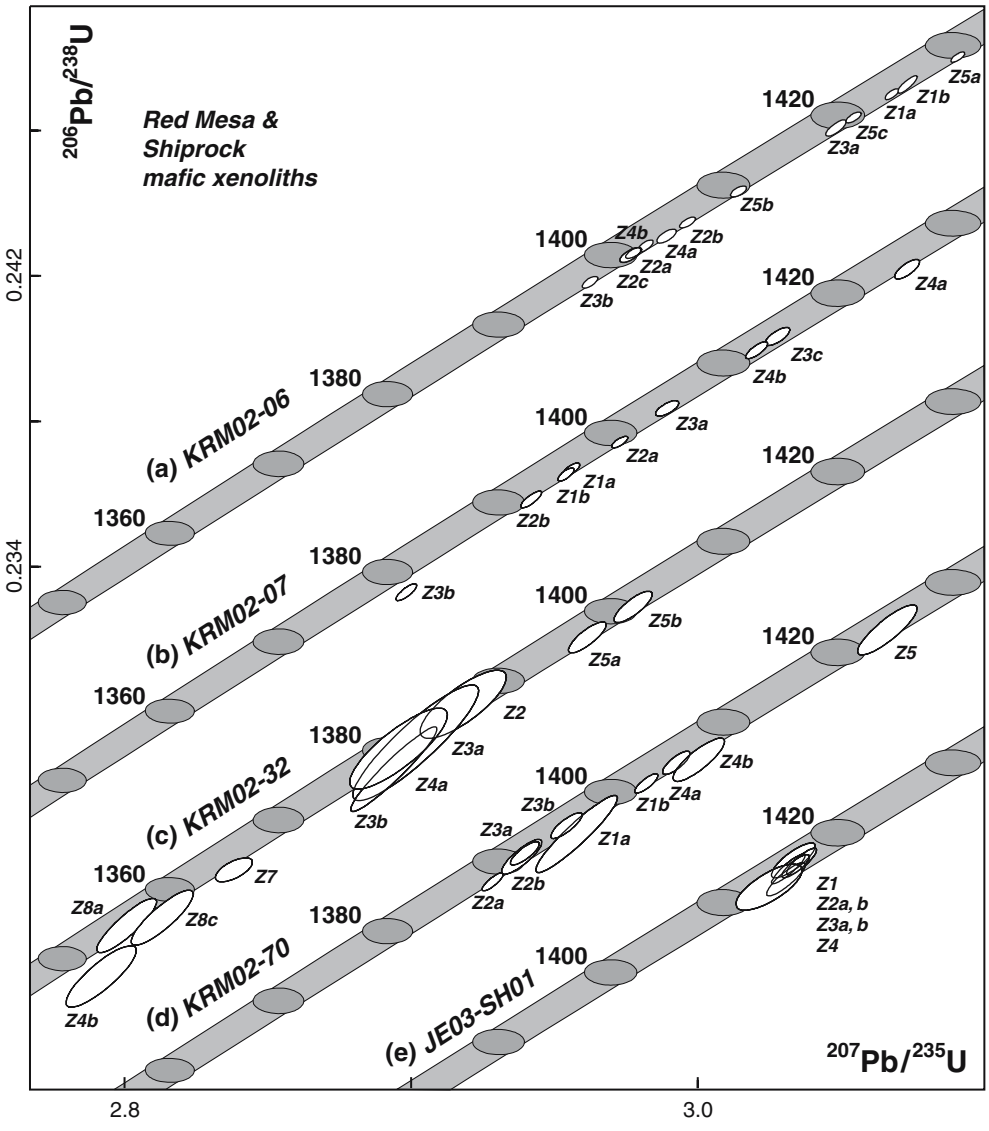

Fig. 4 U–Pb concordia diagram for zircon analyses from mafic xenoliths from Red Mesa and Shiprock diatremes. Labels on error ellipses correspond to zircon grains (*numbers*) and fragments (*letters*) from the same grain. Error ellipses are 2σ. Plotted with Isoplot (Ludwig 2001). Concordia is shown as a *band* that includes the U decay constant errors of Steiger and Jäger (1977). See Table 2 for analytical data

CL-bright and unzoned or have weak patchy and broad concentric zoning (Fig. 2). One-third of the grains have small, CL-dark, elongate (aspect ratio of 5:2) cores with concentric oscillatory zoning. Fragments composed mostly of dark cores are U-richer than fragments without cores (150–180 vs. 50–90 ppm) and Th/U is lower (0.18–0.29 vs. 0.83–1.49). Eleven fragments from five grains yielded concordant to moderately discordant dates (Table 2, Fig. 6a). The oldest dates are from two grains with large dark cores (Z1, Z5). Fragments from moderately bright grains without cores (Z1–Z3) and rim fragments from grains with cores yielded dates of 1,416–1,391 Ma. Six fragments (at least one from each grain) form a poorly fitting discordia with upper and lower intercepts of $1{,}728 \pm 49$ and $1{,}389 \pm 18$ Ma (MSWD = 1.8), respectively. Variable Hf isotopic compositions were obtained from two grains with dates of 1,401 Ma ($\varepsilon_{Hf} = +4.3$ and $+0.7$; $T_{DM} = 1.68$ and 1.82 Ga) (Table 3, Fig. 5).

The Thumb

Felsic granulites

Zircon in felsic granulite xenoliths from The Thumb appear similar to that from Red Mesa with an exception that many grains are tan and pink rather than colorless. Some grains have feathery and curved zoning, others are weakly zoned, and yet others have sector and fine concentric oscillatory zoning (Fig. 2). Nearly every grain in KTT02-07 has an elongate core (aspect ratio of 2:1) with fine concentric oscillatory zoning. In contrast with zircon from Red Mesa, the sector and fine concentric oscillatory-zoned zircon from the Thumb is U-rich (2,300–4,300 ppm) and has low Th/U (0.01–0.11). Zircon lacking sector and fine concentric oscillatory zoning in KTT02-01 is also U-rich with low Th/U, whereas such zircon in KTT02-07 is U-poor (100 ppm) with high Th/U (1.05).

Table 3 Lu–Hf isotopic data

Sample	Zircon type	t (Ga)	ID [Lu] (ppm)	ID [Hf] (ppm)	$^{176}Lu/^{177}Hf$	$^{176}Hf/^{177}Hf$	± (2σ)	ε_{Hf} (t)	T_{DM} (Ga)
KRM02-06 mafic granulite from Red Mesa diatreme									
Z5a	Igneous	1.43	16.88	10,388	0.00023	0.282077	9	7.1	1.60
Z1b	Igneous	1.43	6.53	5,146	0.00018	0.282006	6	4.5	1.69
Z1a	Igneous	1.43	7.93	6,893	0.00016	0.281997	5	4.1	1.71
Z2a	Igneous	1.43	17.05	7,552	0.00032	0.282095	7	7.4	1.58
Z4a	Metamorphic	1.41	4.69	1,970	0.00034	0.282197	26	10.6	1.44
Z4b	Metamorphic	1.41	12.42	4,754	0.00037	0.282196	12	10.5	1.44
KRM02-07 mafic granulite from Red Mesa diatreme									
Z4a	Igneous	1.43	16.42	17,035	0.00014	0.282097	18	7.8	1.57
Z4b	Metamorphic	1.41	23.44	10,872	0.00031	0.281960	28	2.4	1.76
Z1a	Metamorphic	1.40	13.45	4,886	0.00039	0.281916	17	0.4	1.83
KRM02-32 mafic granulite from Red Mesa diatreme									
Z5a	Metamorphic	1.40	1.57	4,326	0.00005	0.282086	8	6.8	1.58
Z2c	Metamorphic	1.39	0.85	2,861	0.00004	0.281890	33	−0.5	1.85
Z4a	Metamorphic	1.38	0.33	1,656	0.00003	0.281886	25	−0.7	1.85
KRM02-69 felsic granulite from Red Mesa diatreme									
Z3	Metamorphic	1.40	4.55	15,472	0.00004	0.282015	16	4.3	1.68
Z4b	Metamorphic	1.40	1.45	5,468	0.00004	0.281912	12	0.6	1.82
KRM02-70 mafic granulite from Red Mesa diatreme									
Z4a	Metamorphic	1.41	3.95	5,679	0.00010	0.282050	19	5.6	1.63
Z1a	Metamorphic	1.40	0.18	840	0.00003	0.282058	18	5.9	1.62
Z3a	Metamorphic	1.39	8.99	31,844	0.00004	0.282085	11	6.6	1.58
KTT02-01 felsic granulite from The Thumb diatreme									
Z6a	Igneous	1.60	41.50	17,973	0.00033	0.281996	7	7.8	1.71
Z6c	Igneous	1.53	63.70	26,934	0.00034	0.282015	4	6.9	1.69
Z6b	Igneous	1.51	38.54	20,128	0.00027	0.282049	5	7.8	1.64
Z4b	Metamorphic	1.40	2.93	8,143	0.00005	0.282262	5	13.0	1.34
Z4c	Metamorphic	1.40	4.05	16,260	0.00004	0.282240	5	12.2	1.37
Z1a	Metamorphic	1.38	3.18	16,004	0.00003	0.282289	6	13.6	1.30
KTT02-07 felsic granulite from The Thumb diatreme									
Z4b	Igneous	1.64	44.51	5,492	0.00115	0.282095	17	11.4	1.61
Z4a	Igneous	1.64	83.07	12,702	0.00093	0.282110	10	12.0	1.58
Z1b	Igneous	1.51	11.41	10,117	0.00016	0.282190	9	12.8	1.44
Z1a	Metamorphic	1.41	7.41	10,326	0.00010	0.282127	5	8.4	1.53
JC03-SH-01 mafic granulite from Shiprock diatreme									
Z1a	Metamorphic	1.42	1.06	7,105	0.00002	0.281901	43	0.6	1.83
Z2a	Metamorphic	1.42	11.98	8,982	0.00019	0.281921	33	1.2	1.81

The quoted uncertainty for the $^{176}Hf/^{177}Hf$ of each sample is the internal standard error; the external reproducibility of the JMC-475 Hf isotope standard during the course of the study was 0.282156 ± 14 (2σ). For calculation of ε_{Hf} values we used present-day $(^{176}Hf/^{177}Hf)_{CHUR} = 0.282772$ and $(^{176}Lu/^{177}Hf)_{CHUR} = 0.0332$ (Blichert-Toft and Albarede 1997); extrapolated initial calculations used $\lambda = 1.865\times10^{-11}$ (Scherer et al. 2001). Depleted mantle model ages utilized present-day $(^{176}Hf/^{177}Hf)_{DM} = 0.283224$, $(^{176}Lu/^{177}Hf)_{DM} = 0.03813$. $t = {}^{207}Pb/^{206}Pb$ zircon date

A search for zircon in thin sections of KTT02-01 was conducted with the electron microprobe to determine the petrographic setting and ascertain whether growth domains found in the large grains from the mineral separates exist in smaller grains that comprise most of the zircon population. Five to ten moderate-sized (> 20 μm) grains were found in each of the four 25×45 mm sections. Two prominent types of CL zoning patterns are also common in the large grains from the mineral separates: CL-dark cores with fine concentric oscillatory zoning surrounded by CL-bright, weakly zoned to unzoned rims (Fig. 7). Zircon occurs in a variety of petrographic settings, including within Grt, Pyx, Qtz, and Pl. Some of the zircon inclusions within Grt have CL-bright, weakly zoned rims (Fig. 7) that may be part of the same generation of zircon as the majority of the CL-bright, weakly zoned grains and rims.

Zircon from The Thumb yielded concordant to moderately discordant dates (Table 2, Fig. 6). In KTT02-01, three fragments from an oscillatory-zoned grain with a narrow bright rim (Z6) and one fragment from a grain with both sector and oscillatory zoning (Z3c) yielded a discordia with upper and lower intercepts of 1,649 ± 27 and 1,382 ± 21 Ma (MSWD = 0.2), respectively. Fragments from the oscillatory-zoned

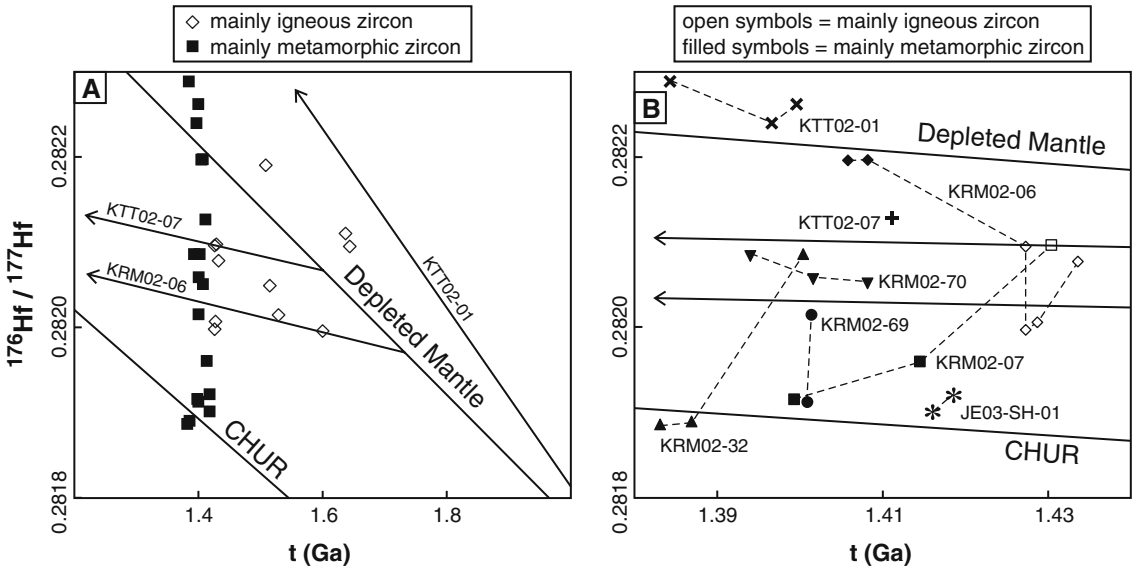

Fig. 5 Hf isotopic data. **a** Data from all zircon grains. Evolution curves for samples KRM02-06, KTT02-01, and KTT02-07 are taken from Lu to Hf whole rock data. Fragments composed mostly of igneous zircon are shown with *open symbols* and those composed mostly of metamorphic zircon are shown with *filled symbols*. **b** Data from zircon fragments with dates of 1.44–1.38 Ga. Fragments from the same xenolith are shown with the same symbol and connected by *dashed lines*. See Tables 3 and 4 for analytical data

grain lie closer to the upper intercept, with the oldest fragment (Z6a) having a $^{207}Pb/^{206}Pb$ date of 1,600 Ma. Other fragments from the sector- and oscillatory-zoned grain (Z3) are concordant near the lower intercept at 1,414 and 1,406 Ma. Two fragments from each of two other CL-bright grains with curved, feathery zoning yielded nearly overlapping dates of 1,398 (Z4) and 1,383 Ma (Z1). One fragment from a bright, unzoned grain (Z5) yielded a slightly older date of 1,420 Ma. In KTT02-07, six fragments from three grains (Z1, Z4, Z5) yielded a poorly fitting discordia with upper and lower intercepts of $1,666 \pm 27$ and $1,393 \pm 22$ Ma (MSWD = 1.8), respectively. A grain consisting mostly of a CL-dark core with oscillatory zoning (Z4) yielded the oldest dates of 1,644 and 1,637 Ma. The youngest fragment is from a bright, weakly zoned grain (Z1a) that is concordant at 1,411 Ma. Other fragments from Z1 yielded older dates that suggest a CL-dark core lies below the imaged grain surface. Two fragments from a grain with a CL-bright oscillatory-zoned inner core and a dark oscillatory zone outer core (Z3) yielded analyses that lie slightly below the discordia line between 1,660 and 1,400 Ma, suggesting that the inner core is > 1,660 Ma.

Table 4 Sm–Nd and Lu–Hf whole rock isotopic data

Sample	Diatreme	ID [Sm] (ppm)	ID [Nd] (ppm)	$^{147}Sm/^{144}Nd$	$^{143}Nd/^{144}Nd$	± (2σ)	ε_{Nd} (0)	ε_{Nd} (1.4)	T_{DM} (Ga)
KRM02-06	Red Mesa	5.8752	29.8138	0.11914	0.512031	4	−11.84	2.08	1.80
KTT02-01	The Thumb	1.7851	5.1630	0.20903	0.512928	6	5.66	3.46	7.13
KTT02-07	The Thumb	3.4492	16.7937	0.12417	0.512112	6	−10.25	2.77	1.76

Sample	Diatreme	ID [Lu] (ppm)	ID [Hf] (ppm)	$^{176}Lu/^{177}Hf$	$^{176}Hf/^{177}Hf$	± (2σ)	ε_{Hf} (0)	ε_{Hf} (1.4)	T_{DM} (Ga)
KRM02-06	Red Mesa	0.5034	7.7007	0.00928	0.282276	5	−17.55	4.84	1.73
KTT02-01	The Thumb	0.7311	1.9018	0.05456	0.283887	8	39.44	19.51	2.12
KTT02-07	The Thumb	0.3725	5.9819	0.00884	0.282335	6	−15.45	7.36	1.60

The quoted uncertainty for the $^{143}Nd/^{144}Nd$ of each sample is the internal standard error; the external reproducibility of the JNdi-1 standard over the course of the study was 0.512098 ± 9 (2σ); uncertainty in [Sm], [Nd] and $^{147}Sm/^{144}Nd$ are estimated at ≤ 0.2% (2σ). Calculation of ε_{Nd} values used present-day $(^{143}Nd/^{144}Nd)_{CHUR} = 0.512638$ and $(^{147}Sm/^{144}Nd)_{CHUR} = 0.1967$; extrapolated initial calculations used $\lambda = 6.54 \times 10^{-12}$ (Lugmair and Marti 1978). Depleted mantle model ages used a linear growth model with present-day $(^{143}Nd/^{144}Nd)_{DM} = 0.513151$, $(^{147}Sm/^{144}Nd)_{DM} = 0.2137$

The quoted uncertainty for the $^{176}Hf/^{177}Hf$ of each sample is the internal standard error; the external reproducibility of the JMC-475 standard over the course of the study was 0.282156 ± 14 (2σ). Uncertainty in [Lu], [Hf] and $^{176}Lu/^{177}Hf$ are estimated at ≤ 0.2% (2σ). Calculation of ε_{Hf} values used present-day $(^{176}Hf/^{177}Hf)_{CHUR} = 0.282772$ and $(^{176}Lu/^{177}Hf)_{CHUR} = 0.0332$ (Blichert-toft and Albarede 1997); extrapolated initial calculations used $\lambda = 1.865 \times 10^{-11}$ (Scherer et al. 2001). Depleted mantle model ages used a linear growth model with present-day $(^{176}Hf/^{177}Hf)_{DM} = 0.283224$, $(^{176}Lu/^{177}Hf)_{DM} = 0.03813$

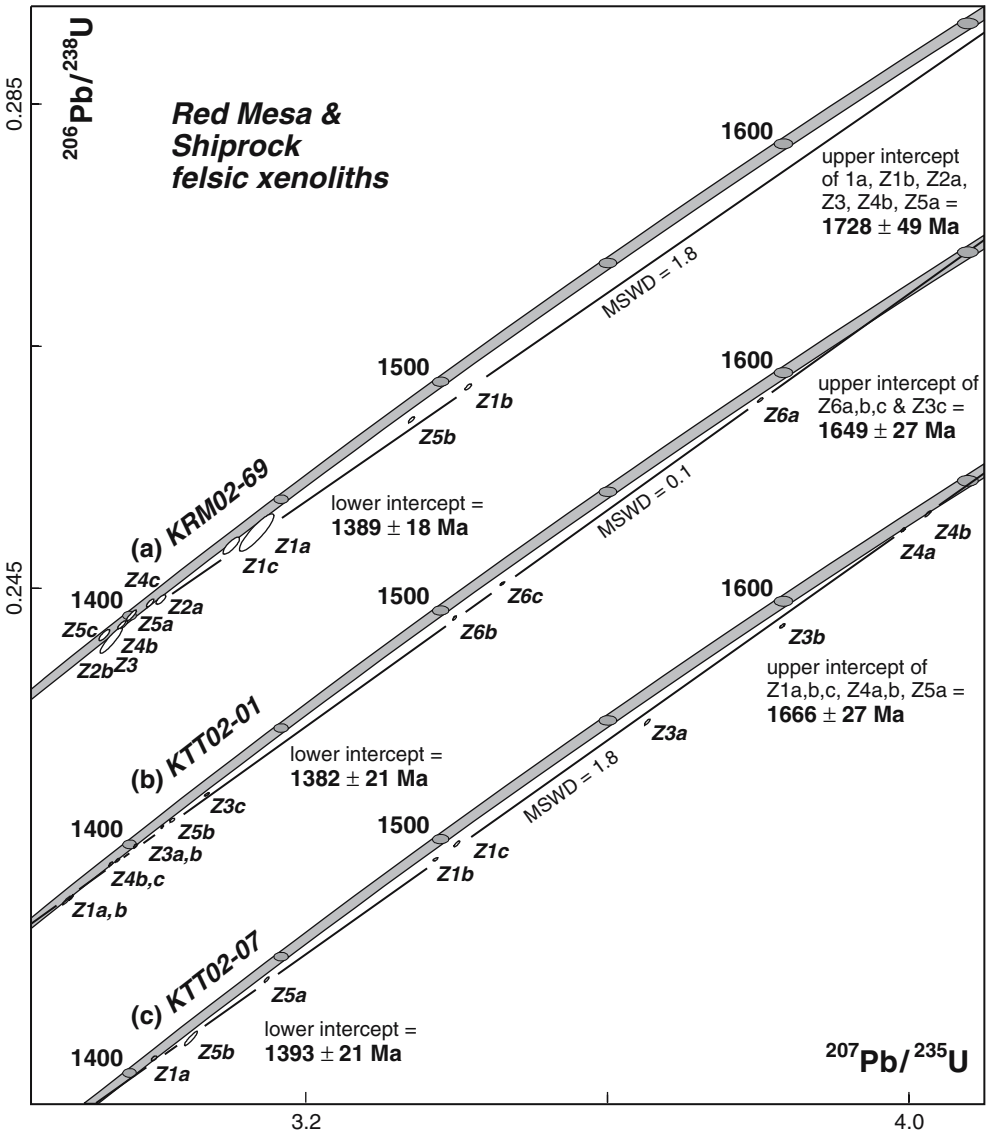

Fig. 6 U–Pb concordia diagram for zircon analyses from felsic xenoliths from Red Mesa and The Thumb diatremes. Error ellipses are 2σ. Plotted with Isoplot (Ludwig 2001). Concordia is shown as a *band* that includes the U decay constant errors of Steiger and Jäger (1977). See Table 2 for analytical data

Hf isotopic compositions were measured in three grains from KTT02-01, including multiple fragments from two grains (Table 3, Fig. 5). Fragments from the same grain that have variable proportions of ~1.65 and 1.38 Ga zircon have covarying Hf isotope compositions; the fragment with the highest proportion ~1.65 Ga zircon has the least radiogenic measured value ($\varepsilon_{Hf} = +6.9$–$+7.8$; $T_{DM} = 1.71$–1.64 Ga) and two young grains (1,400 and 1,384 Ma) have the most radiogenic compositions measured in this study ($\varepsilon_{Hf} = +12.2$–$+13.6$; $T_{DM} = 1.37$–1.30 Ga). Lu–Hf and Sm–Nd whole rock data from KTT02-07 are similar to those from KRM02-6 (Table 4). Hf isotopic compositions were analyzed from two fragments from each of two grains from KTT02-07 (Table 3, Fig. 5). Fragments of one grain that is mostly composed of ~1.64 Ga zircon have radiogenic initial Hf isotope compositions ($\varepsilon_{Hf} = +11.4$–$+12.0$; $T_{DM} = 1.61$–1.58 Ga). Two fragments of the other grain have differing Hf isotope compositions; a mixed core-rim fragment has a relatively radiogenic composition similar to the mixed grains from KTT02-01, and a fragment apparently composed entirely of 1,411 Ma zircon has an unradiogenic composition ($\varepsilon_{Hf} = +8.4$; $T_{DM} = 1.53$ Ga).

Shiprock

A mafic granulite xenolith from Shiprock (JE03-SH-0) has zircon similar to that from Red Mesa mafic xenoliths. Most grains are CL-bright with weak zoning, and one-third of the grains have small CL-dark, complexly zoned cores. Six fragments from four grains without cores yielded concordant dates (Table 2, Fig. 4e) with a weighted mean age of 1,417.8 ± 1.0 Ma (MSWD = 1.2). Hf isotopic compositions of two of the fragments are unradiogenic ($\varepsilon_{Hf} = +0.6$ and $+1.2$; $T_{DM} = 1.83$ and 1.81 Ga) (Table 3, Fig. 5).

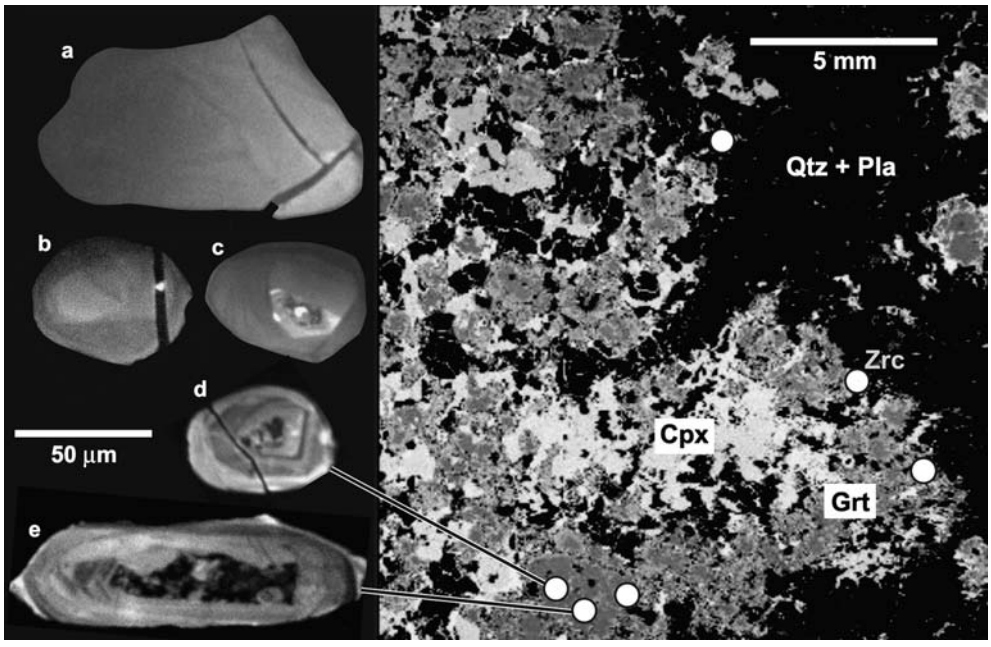

Fig. 7 Images of in situ zircon grains in xenolith KTT02-01 found during compositional mapping by the electron microprobe. Zircon (*white circle*) is shown relative to the main mineral phases (*bright* Cpx; *intermediate* Grt; *dark* Qtz and Pl) in a Mg Kα map (*right*). CL images of grains (*left*) that exist within the section are d (inclusion within Grt) and e (lies in altered zone between Grt crystals). Grains a–c exist elsewhere in the section. Mineral abbreviations after Kretz (1983)

Discussion

Lower crustal magmatism

1.73–1.65 Ga Felsic xenoliths

Zircon cores and some whole grains in the felsic granulite xenoliths are prismatic and elongate (aspect ratios of 2:1–5:2) with concentric oscillatory zoning (Fig. 2). They are generally U-rich compared with the CL-bright grains and rims in the same xenoliths, and Th/U is much lower. These characteristics, combined with the felsic composition of the xenoliths, suggest that this zircon formed during igneous crystallization of the protolith granitoid rocks. The protolith ages from Red Mesa and The Thumb are ~1.73 and 1.65 Ga, respectively, within the range of Nd whole rock model ages from lower crustal granulite and Grt amphibolite xenoliths from the Navajo volcanic field (Wendlandt et al. 1993). Ages of middle and upper crustal metagranitoid and granitoid xenoliths from the

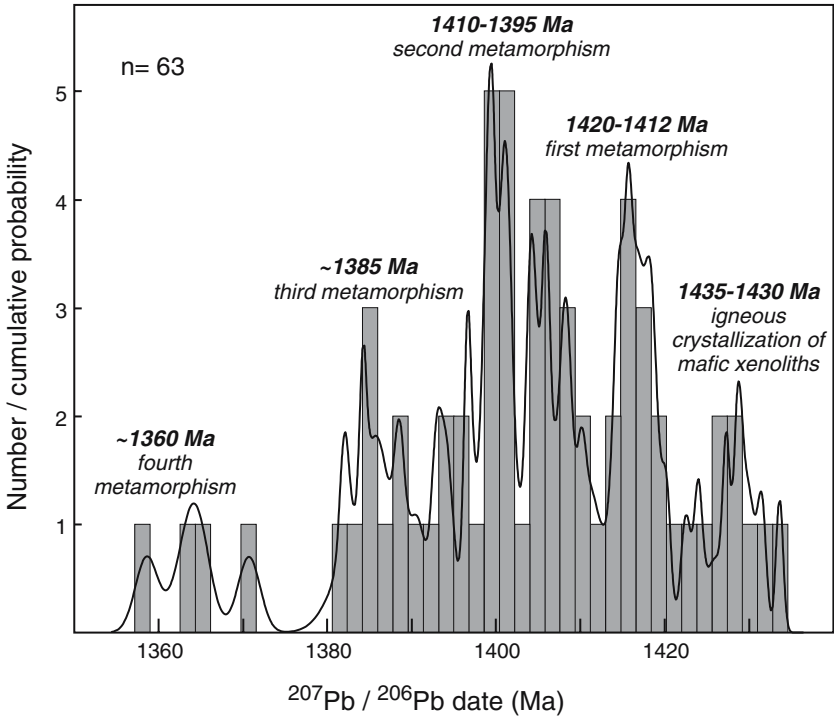

Fig. 8 Histogram and cumulative probability plots of $^{207}Pb/^{206}Pb$ dates from zircons that lack 1.7–1.6 Ga cores. Bin width is 1.7 myr, the average 2σ error on the $^{207}Pb/^{206}Pb$ dates

Navajo field (Condie et al. 1999) are similar to the 1.73 Ga Red Mesa xenolith. In basement rocks around the Colorado Plateau, 1.73 Ga granitoid rocks are more common than 1.65 Ga rocks (Karlstrom and Bowring 1993).

U–Pb dates from igneous zircon in two felsic xenoliths from The Thumb are coeval with the Hf depleted mantle model ages measured in the same grains and with Hf and Nd whole rock depleted mantle model ages from one of these xenoliths. The agreement between U and Pb crystallization ages and source model dates supports our interpretation that the zircon formed in the protolith magma. No evidence exists for the interaction between protolith magmas and the significantly older (>1.8 Ga) crust.

1.43 Ga Mafic xenoliths

Zircon from three of the four mafic granulites have CL-dark cores surrounded by CL-bright rims (Fig. 2). The cores have concentric oscillatory zoning and sector zoning that is typical of zircon crystallized from mafic magmas (Rubatto and Gebauer 2000), and thus are interpreted as having formed during crystallization of a protolith magma. The oldest core fragments, which presumably contain little or no CL-bright rim, yield ~1,430 Ma dates. A metamorphic origin is not favored because the cores differ greatly in U concentration and zoning from the CL-bright domains that are interpreted as being metamorphic (see below) and the 1.7–1.6 Ga felsic xenoliths do not record zircon growth at ~1,430 Ma. Ages of ~1.4 Ga are common among middle and upper crustal metagranitoid and granitoid xenoliths from the Navajo field (Condie et al. 1999) and basement rocks around the Colorado Plateau. Mafic plutonic rocks with ages of ~1.4 Ga are less common (Karlstrom and Bowring 1993).

U–Pb zircon dates from mafic xenoliths from Red Mesa are significantly younger than the Hf depleted mantle model ages measured in the same grains, which are coeval with Hf and Nd whole rock depleted mantle model ages from one mafic xenolith. This age discrepancy is strong evidence that the magmatic precursors of the xenoliths were substantially contaminated by 1.7–1.6 Ga crust, some of which may be similar to the felsic xenoliths from Red Mesa and The Thumb.

Lower crustal metamorphism

Cathodoluminescence-bright zircon rims and whole grains have weak sector, curved, and feathery zoning (Fig. 2) that is typical of metamorphic zircon (Hanchar and Rudnick 1995; Rubatto and Gebauer 2000; Corfu et al. 2003). The metamorphic domains contrast greatly with the CL-dark igneous cores (see above); metamorphic domains are U-poor (<240 ppm) with higher Th/U (0.20–1.49). It is likely that some of the metamorphic domains grew during the granulite facies event that formed the primary assemblage of Pyx–Grt–Pl. Petrographic evidence for this conclusion is found in a xenolith from The Thumb (KTT02-01) in which the common association of zircon with Grt that lies between Cpx and Pl (Fig. 7) suggests that it grew during the breakdown of Cpx and the formation of Grt and new Pl. Estimates of 1.3 GPa and 800°C, interpreted to represent conditions during the granulite event, were made from xenoliths from The Thumb (Fig. 3), and similar estimates of 1.15 GPa and 780°C were made from a mafic granulite from Red Mesa (Selverstone et al. 1999).

Metamorphic domains that we attempted to isolate from igneous cores yielded dates that cluster at ~1,420–1,412, 1,410–1,395, 1,385, and 1,360 Ma (Fig. 8). Zircon growth at 1,417.8 ± 1.0 Ma in the xenolith from Shiprock (JE03-SH-01) is apparently the oldest episode of metamorphic recrystallization. Domains with dates of 1,410–1,395 Ma are most prevalent, existing in all samples except the Shiprock xenolith, and may record the main episode of granulite facies metamorphism. The 1,385 Ma domains, found only in two xenoliths, record a third episode of metamorphic growth, while a fourth episode is suggested by a few 1,360 Ma dates in one xenolith. Dates of >1,420 Ma are mostly from grains with visible igneous cores, suggesting that the analyzed fragments are likely mixtures of >1,430 Ma igneous cores and <1,420 Ma metamorphic rims. Some fragments from the same grain yielded identical dates, yet many differ by at least a few million years (Fig. 4). The spread in dates between 1,410 and 1,395 Ma probably indicates that most grains are composites of domains formed during this period. The substantial variability of Hf depleted mantle model ages (T_{DM} = 1.8–1.3 Ga) within and between zircon from xenoliths is taken as evidence that metamorphic zircon grew from a variety of introduced fluid compositions or from different aged minerals with diverse time-integrated Lu/Hf ratios.

Timing of metamorphism and tectonic models

Selverstone et al. (1999) used differences in xenolith rock types, *P–T* paths, and alteration histories to suggest that the Mazatzal and Yavapai provinces were juxtaposed along a boundary that lies within the Navajo volcanic field, separating diatremes to the northwest from those to the southeast. They proposed that this subduction model could be tested by more detailed work in basement rocks around the Colorado Plateau and through additional geochronological study of xenoliths. Our U–Pb zircon data from lower crustal xenoliths do not directly date the eclogitic metamorphism or hydrous alteration that are crucial to this model. In fact, five of the six dated xenoliths that contain protolith igneous zircon formed after the proposed subduction at 1.75–1.70 Ga. However, our data constrain the timing of the youngest metamorphism and subsequent alteration.

Because it is likely that the products of hydrous alteration during subduction would have been overprinted by the 1.4 Ga granulite facies metamorphism recorded by zircon, the alteration that forms a crucial part of the model of Selverstone et al. (1999) probably occurred at or after 1.4 Ga, postdating the collision by several hundred million years. In addition, *P–T* paths that were used to support this model may instead partly record equilibrium or re-equilibration at 1.4 Ga. Recognition of an important 1.4 Ga metamorphism in the lower crust leaves the restricted occurrence of eclogite xenoliths from the northwest diatremes as the only evidence for the subduction model. However, two studies that dated zircon from eclogitic xenoliths from the Navajo field suggested that eclogite formed during Late Cretaceous to Tertiary subduction rather than in the Proterozoic. Usui et al. (2003) concluded that the protoliths of the eclogites are part of the subducted Farallon plate that formed in the Late Cretaceous and underwent subduction-related metamorphism shortly afterward. Smith et al. (2004) concluded that the eclogite protoliths are Mesoproterozoic mantle rocks that were recrystallized during Late Cretaceous to Tertiary subduction.

Basaltic underplate?

Zircon data from mafic granulite xenoliths indicate that ~1,435 Ma mafic magmas crystallized before the growth of ~1,420–1,360 Ma metamorphic zircon, at least some of which formed during granulite facies metamorphism (1.3 GPa and 800°C) in the lower crust beneath the Colorado Plateau. Hf isotopic data from zircon indicate that protoliths of the mafic xenoliths interacted with 1.7–1.6 Ga crust. These findings can be used to support the existence of a ~1.4 Ga basaltic underplate as proposed by Karlstrom et al. (1997, 2002). However, the volume of 1.4 Ga mafic rocks in the lower crust is unknown and the time lag of ~15 myr between igneous crystallization and the earliest metamorphic episode suggests there was a protracted period of lower crustal heating and metamorphism that lasted at least 60 myr (time span between oldest metamorphic zircon in Shiprock and youngest metamorphic zircon from Red Mesa). The protracted nature of this "event" in the lower crust is consistent with the timescale of granitic magmatism in the middle and upper crusts and must be accounted for in any model for the generation of these granitoids. Additional integrated geochemical, geochronological, and isotopic studies of the xenoliths are required to understand the interplay between magmatism and metamorphism in the lower crust.

Summary

The age, composition, and thermal history of the lower crust in southwestern Laurentia are key for understanding the processes of Proterozoic lithospheric growth, modification, and reactivation. Xenoliths of mafic and felsic granulite are interpreted to have been derived from the lower crust based on the primary mineralogy of Cpx–Grt–Pl ± Qtz and thermobarometry estimates of ~1.3 GPa and 800°C. Metamorphic zircon grains yield U–Pb dates of 1,420–1,414, 1,410–1,395 (most prevalent), 1,385, and 1,360 Ma. The significant variability within and between xenoliths in zircon initial Hf isotopic compositions ($\varepsilon_{Hf} = -0.7$ to $+13.6$) and depleted mantle model ages ($T_{DM} = 1.8$–1.3 Ga) indicates growth from different aged sources with diverse time-integrated Lu/Hf ratios. Xenoliths also contain oscillatory- and sector-zoned zircon cores and whole grains that likely grew during igneous crystallization of the protoliths. Igneous cores in the felsic xenoliths have U–Pb ages of ~1,730 and 1,650 Ma and generally unradiogenic Hf isotopic compositions ($\varepsilon_{Hf} = +6.9$–$+7.8$, $T_{DM} = 1.7$–1.6 Ga), consistent with the protoliths being derived from "juvenile" Proterozoic crust. Igneous cores in zircon from mafic xenoliths have U–Pb dates of ~1,435 Ma and unradiogenic Hf isotopic compositions ($\varepsilon_{Hf} = +4.1$–$+7.8$, $T_{DM} = 1.7$–1.6 Ga), consistent with mafic magmas having interacted with older crust. These results suggest a strong link between 1.4 Ga mafic magmatism and metamorphism in the lower crust and granitic magmatism and metamorphism in the exposed middle crust.

Acknowledgements We are grateful to S. Semken for guiding us around the Four Corners area and for facilitating xenolith collection. We thank the Minerals Branch of the Navajo Nation for allowing us to collect samples. This work was supported by Continental Dynamics Program grants (EAR-000351 to SAB, EAR-0003500 and EAR-0208473 to KEK, and EAR-0003459 to MLW). Comments from two anonymous reviewers improved the clarity of the manuscript.

References

Bennett VC, DePaolo DJ (1987) Proterozoic crustal history of the western United States as determined by neodymium isotopic mapping. Geol Soc Am Bull 99:674–685

Berman RG (1991) Thermobarometry using multi-equilibrium calculations: a new technique, with petrological applications. Can Mineral 29:833–855

Berman RG, Aranovich LY (1996) Optimized standard state and solution properties of minerals. I. Model calibration for olivine, orthopyroxene, cordierite, garnet and ilmenite in the system FeO–MgO–CaO–Al_2O_3–TiO_2–SiO_2. Contrib Mineral Petrol 126:1–24

Berman RG, Brown TH (1992) Thermobarometry with estimation of equilibration state (TWEEQU): a software package for IBM or compatible personal computers. Open File Report, Geological Survey of Canada, 2534

Blichert-Toft J, Albarede F (1997) The Lu–Hf isotope geochemistry of chondrites and the evolution of the mantle–crust system. Earth Planet Sci Lett 148:243–258

Bowring SA, Karlstrom KE (1990) Growth, stabilization, and reactivation of Proterozoic lithosphere in the Southwestern United States. Geology 18:1203–1206

Chen YD, O'Reilly SY, Kinny PD, Griffin WL (1994) Dating lower crust and upper mantle events: an ion microprobe study of xenoliths from kimberlitic pipes, South Australia. Lithos 32:77–94

Condie KC (1992) Proterozoic terranes and continental accretion in southwestern United States. In: Condie KC (ed) Proterozoic crustal evolution. Amsterdam, Elsevier, pp 447–480

Condie KC, Latysh N, Van Schmus WR, Kozuch M, Selverstone J (1999) Geochemistry, Nd and Sr isotopes, and U/Pb zircon ages of granitoid and metasedimentary xenoliths from the Navajo volcanic field, Four Corners area, Southwestern United States. Chem Geol 156:95–133

Corfu F, Hanchar JM, Hoskin PWO, Kinny P (2003) Atlas of zircon textures. In: Hanchar JM, Hoskin PWO (eds) Zircon. Reviews in mineralogy and geochemistry. Mineral Soc Am, vol 53, pp 468–500

Davis WJ (1997) U–Pb zircon and rutile ages from granulite xenoliths in the Slave Province: evidence for mafic magmatism in the lower crust coincident with Proterozoic dike swarms. Geology 25:343–346

Davis WJ, Canil D, MacKenzie JM, Carbno GB (2003) Petrology and U–Pb geochronology of lower crustal xenoliths and the development of a craton, Slave Province, Canada. Lithos 71:541–573

Farmer GL, Bowring SA, Williams ML, Christensen NI, Matzel JP, Stevens L (2005) Contrasting lower crustal evolution across an archean-proterozoic suture: physical, chemical and geochronologic studies of lower crustal xenoliths in southern Wyoming and northern Colorado. In: Keller GR, Karlstrom KE (eds) Lithospheric structure and evolution of the rocky mountains. American Geophysical Union Monograph, pp 139–162

Frost CD, Frost BR (1997) Reduced rapakivi-type granites: the tholeittic connection. Geology 25:647–650

Grambling JA, Dallmayer RD (1993) Tectonic evolution of Proterozoic rocks in the Cimarron Mountains, northern New Mexico. J Meta Geol 11:739–755

Hanchar JM, Rudnick RL (1995) Revealing hidden structures: the application of cathodoluminescence and back-scattered electron imaging to dating zircons from lower crustal xenoliths. Lithos 36:289–303

Hawkins DP, Bowring SA, Ilg BR, Karlstrom KE, Williams ML (1996) U–Pb geochronologic constraints on the Paleoproterozoic crustal evolution of the Upper Granite Gorge, Grand Canyon, Arizona. Geol Soc Am Bull 108:1167–1181

Hodges KV, Bowring SA (1995) $^{40}Ar/^{39}Ar$ thermochronology of isotopically zoned micas: insights from the southwestern USA Proterozoic orogen. Geochim Cosmochim Acta 59:3205–3220

Hodges KV, Hames WE, Bowring SA (1994) $^{40}Ar/^{39}Ar$ age gradients in micas from a high-temperature–low-pressure metamorphic terrain; evidence for very slow cooling and implications for the interpretation of age spectra. Geology 22:55–58

Karlstrom KE, Bowring SA (1988) Early Proterozoic assembly of tectonostratigraphic terranes in southwestern North America. J Geol 96:561–576

Karlstrom KE, Bowring SA (1993) Proterozoic orogenic history of Arizona. In: Read JC Jr et al (ed) Precambrian, onterminous U.S. (Decade of North American Geology, v. C-2). Geol Soc Am, Boulder, pp 118–211

Karlstrom KE, CD-ROM Working Group (2002) Structure and evolution of the lithosphere beneath the Rocky Mountains: initial results. GSA Today 12:4–9

Karlstrom KE, Amato JM, Williams ML, Heizler M, Shaw C, Read A, Bauer P (2006) Proterozoic tectonic evolution of the New Mexico region: a synthesis. In: Geology of New Mexico. New Mexico Geological Society Memoir (in press)

Karlstrom KE, Dallmeyer RD, Grambling JA (1997) $^{40}Ar/^{39}Ar$ evidence for 1.4 Ga regional metamorphism in New Mexico; implications for thermal evolution of lithosphere in the Southwestern USA. J Geol 105:205–223

Kay RW, Kay SM (1993) Delamination and delamination magmatism. Tectonophysics 219:177–189

Kretz R (1983) Symbols for rock forming minerals. Am Mineral 68:277–279

Krogh TE (1982) Improved accuracy of U–Pb ages by the creation of more concordant systems using an air abrasion technique. Geochim Cosmochim Acta 46:637–649

Laughlin A, Aldrich M, Shafiquillah M, Husler J (1986) Tectonic implications of the age, composition, and orientation of lamprophyre dikes, Navajo volcanic field, Arizona. Earth Planet Sci Lett 76:361–374

Ludwig KR (1980) Calculation of uncertainties of U–Pb isotope data. Earth Planet Sci Lett 46:212–220

Ludwig KR (2001) Isoplot/Ex: a geochronological toolkit for microsoft excel. Berkeley Geochronology Center. Special Publication No. 1a (rev. 2.49)

Lugmair GW, Marti K (1978) Lunar initial $^{143}Nd/^{144}Nd$: differential evolution of the lunar crust and mantle. Earth Planet Sci Lett 39:349–357

Mattie PD, Condie KC, Selverstone J, Kyle PR (1997) Origin of the continental crust in the Colorado Plateau; geochemical evidence from mafic xenoliths from the Navajo volcanic field, Southwestern USA. Geochim Cosmochim Acta 61:2007–2021

McGetchin TR, Smith D, Ehrenberg SN, Roden M, Wilshire HG (1977) Navajo kimberlites and minettes. In: Second international Kimberlite conference field excursion guide, Santa Fe, p 40

Moser DE, Heaman LM (1997) Proterozoic zircon growth in Archean lower crustal xenoliths, southern superior craton—a consequence of Matachewan ocean opening. Contrib Mineral Petrol 128:164–175

Muenker C, Weyer S, Mezger K, Rehkaemper M, Wombacher F, Bischoff A (2000) ^{92}Nb–^{92}Zr and the early differentiation history of planetary bodies. Science 289:1538–1542

Patchett PJ, Tatsumoto M (1980) Lu–Hf total-rock isochron for the eucrite meteorites. Nature 288:571–574

Pedrick JN, Karlstrom KE, Bowring SA (1998) Reconciliation of conflicting tectonic models for Proterozoic rocks of northern New Mexico. J Meta Geol 16:687–707

Pouchou JL, Pichoir F (1985) ''PAP'' phi-rho-Z procedure for improved quantitative microanalysis. In: Armstrong JL (ed) Microbeam analysis. San Francisco Press Inc., San Francisco, pp 104–106

Read A, Karlstrom KE, Grambling JA, Bowring SA, Heizler M, Daniel C (1999) A mid-crustal cross section from the Rincon Range, northern New Mexico: evidence for 1.68 Ga pluton-influenced tectonism and 1.4 Ga regional metamorphism. Rocky Mountain Geol 34:67–91

Rubatto D, Gebauer D (2000) Use of cathodoluminescence for U–Pb zircon dating by ion microprobe: some examples from the Western Alps. In: Pagel M, Barbin V, Blanc P, Ohnenstetter D (eds) Cathodoluminescence in geosciences. Springer, Berlin Heidelberg New York, pp 373–400

Rudnick RL, Williams IS (1987) Dating the lower crust by ion microprobe. Earth Planet Sci Lett 85:145–161

Scherer E, Muenker C, Mezger K (2001) Calibration of the lutetium–hafnium clock. Science 293:683–687

Schmitz MD, Bowring SA (2001) The significance of U–Pb zircon dates in lower crustal xenoliths from the southwestern margin of the Kaapvaal craton, southern Africa. Chem Geol 172:59–76

Schmitz MD, Bowring SA (2003a) Ultrahigh-temperature metamorphism in the lower crust during Neoarchean Ventersdorp rifting and magmatism, Kaapvaal Craton, southern Africa. Geol Soc Am Bull 115:533–548

Schmitz MD, Bowring SA (2003b) Constraints on the thermal evolution of continental lithosphere from U–Pb accessory mineral thermochronology of lower crustal xenoliths, southern Africa. Contrib Mineral Petrol 144:592–618

Schmitz MD, Bowring SA, de Wit MJ, Gartz V (2004) Subduction and terrane collision stabilize the western Kaapvaal craton tectosphere 2.9 billion years ago. Earth Planet Sci Lett 222:363–376

Schoene B, Crowley JL, Condon DJ, Schmitz MD, Bowring SA (2006) Reassessing the U and ^{40}K decay constants for geochronology: new insights from high-precision ID-TIMS U–Pb data. Geochim Cosmochim Acta (in press)

Selverstone J, Pun A, Condie KC (1999) Xenolithic evidence for Proterozoic crustal evolution beneath the Colorado Plateau. Geol Soc Am Bull 111:590–606

Semken S (2003) Black rocks protruding up: the Navajo volcanic field. New Mexico Geol Soc Guidebook 54:133–138

Shaw CA, Karlstrom KE, Williams ML, Jercinovic MJ, McCoy AM (2001) Electron-microprobe monazite dating of ca. 1.71–1.63 Ga and ca. 1.45–1.38 Ga deformation in the Homestake shear zone, Colorado: origin and early evolution of a persistent intracontinental tectonic zone. Geology 29:739–742

Shaw CA, Heizler MT, Karlstrom KE (2005) $^{40}Ar/^{39}Ar$ thermochronologic record of 1.45–1.35 intracontinental orogeny in the southern Rocky Mountains: the role of conductive and advective heating in controlling mid-crustal tectonic styles beneath orogenic plateaus. In: Keller GR, Karlstrom KE (eds) Lithospheric structure and evolution of the Rocky Mountains. American Geophysical Union Monograph, pp 163–184

Silver LT (1965) Mazatzal orogeny and tectonic episodicity. Geol Soc Am Spec Paper 82:185–186

Smith D, Griffin WL (2005) Garnetite xenoliths and mantle–water interactions below the Colorado Plateau, southwestern United States. J Petrol 46:1901–1924

Smith D, Connelly JN, Manser K, Moser DE, Housh TB, McDowell FW, Mack LE (2004) Evolution of Navajo eclogites and hydration of the mantle wedge below the Colorado Plateau, southwestern United States. Geochem Geophys Geosyst 5:Q04005

Steiger RH, Jäger E (1977) Subcommission on geochronology: convention on the use of decay constants in geo- and cosmochronology. Earth Planet Sci Lett 36:359

Usui T, Nakamura E, Kobayashi K, Maruyama S, Helmstaedt H (2003) Fate of the subducted Farallon plate inferred from eclogite xenoliths in the Colorado Plateau. Geology 31:589–592

Wendlandt E, DePaolo DJ, Baldridge WS (1993) Nd and Sr isotope chronostratigraphy of Colorado Plateau lithosphere; implications for magmatic and tectonic underplating of the continental crust. Earth Planet Sci Lett 116:23–43

Wendlandt E, DePaolo DJ, Baldridge WS (1996) Thermal history of Colorado Plateau lithosphere from Sm–Nd mineral geochronology of xenoliths. Geol Soc Am Bull 108:757–767

Williams ML, Karlstrom KE (1997) Looping *P–T* paths and high-*T*, low-*P* middle crust metamorphism: Proterozoic evolution of the southwestern United States. Geology 105:205–223

Williams ML, Jercinovic MJ, Terry M (1999) Age mapping and dating of monazite on the electron microprobe: deconvoluting multistage tectonic histories. Geology 27:1023–1026

Williams ML, Melis EA, Kopf C, Hanmer S (2000) Microstructural tectonometamorphic processes and the development of gneissic layering: a mechanism for metamorphic segregation. J Meta Geol 18:41–57

York D (1969) Least squares fitting of a straight line with correlated errors. Earth Planet Sci Lett 5:320–324